

Coastal sand budget for Southern Pegasus Bay

Stage B: Future sand budget

Prepared for Christchurch City Council

June 2018

Prepared by:

D M Hicks
R Measures
R Gorman

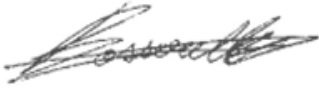


For any information regarding this report please contact:

Murray Hicks
Group Manager - Principal Scientist
Sediment Processes
+64 343 7872
murray.hicks@niwa.co.nz

National Institute of Water & Atmospheric Research Ltd
PO Box 8602
Riccarton
Christchurch 8011

Phone +64 3 348 8987

NIWA CLIENT REPORT No: 2018172CH
Report date: June 2018
NIWA Project: CCC18501

Quality Assurance Statement		
	Reviewed by:	Dr Cyprien Bosserelle
	Formatting checked by:	Fenella Falconer
	Approved for release by:	Dr Jo Hoyle

© All rights reserved. This publication may not be reproduced or copied in any form without the permission of the copyright owner(s). Such permission is only to be given in accordance with the terms of the client's contract with NIWA. This copyright extends to all forms of copying and any storage of material in any kind of information retrieval system.

Whilst NIWA has used all reasonable endeavours to ensure that the information contained in this document is accurate, NIWA does not give any express or implied warranty as to the completeness of the information contained herein, or that it will be suitable for any purpose(s) other than those specifically contemplated during the Project or agreed by NIWA and the Client.

Contents

Executive summary	7
1 Introduction	10
1.1 Background and objectives.....	10
1.2 Summary of current sand budget.....	11
2 Methods.....	13
2.1 Climate change effects on Waimakariri River supply of beach-grade sand	13
2.1.1 Waimakariri sand load change associated with hydrological change.....	13
2.1.2 Human response effects.....	16
2.1.3 Sand entrapment in the tidal reach of the Waimakariri River and Brooklands Lagoon	16
2.2 Effects of wave climate change and sea-level rise	16
2.2.1 Overview.....	16
2.2.2 Future sea-level	17
2.2.3 Changes to the wave climate	17
2.2.4 SWAN modelling scenarios.....	21
2.2.5 Changes in longshore transport potential and beach-profile closure depth	22
2.2.6 Avon-Heathcote Estuary tidal prism and sand entrapment.....	22
2.3 Potential effects of a major earthquake on the Waimakariri River sand delivery .	23
2.3.1 Landslide scenarios.....	23
2.3.2 Time-scale and amount of landslide sand delivery to the coast.....	23
2.3.3 Limitations, including potential sediment retention in landslide lakes ..	25
2.4 Impacts of future sand budget changes on future beach volumes and shoreline position	26
2.4.1 Model development.....	26
2.4.2 Model application	28
2.5 Effects of future sand budget changes on river and estuary mouth stability and coastal flooding.....	28
3 Results	30
3.1 Climate change effects on Waimakariri River supply of beach sand.....	30
3.1.1 Projected annual suspended loads from TopNet modelling coupled with climate change scenarios	30
3.1.2 Changes in Kidson Weather Types	34
3.1.3 Regional projections of hydrological change from national guidance documents.....	35
3.1.4 Changes in land cover.....	37

3.1.5	Changes in gravel extraction rates	37
3.1.6	Changes in sand diversion with irrigation water abstraction.....	38
3.1.7	Sand entrapment in the tidal reach of the Waimakariri River	39
3.1.8	Review of Tonkin & Taylor (2017) assessment	39
3.1.9	Summary of climate change effects on coastal sand delivery	40
3.2	Effects of wave climate change and sea-level rise	41
3.2.1	Changes to nearshore waves and longshore transport potential.....	41
3.2.2	Changes in closure depth	47
3.2.3	Avon-Heathcote Estuary tidal prism and sand entrapment.....	48
3.2.4	Effects on shore stability at the Avon-Heathcote inlet	50
3.3	Potential effects of a major earthquake on the Waimakariri River sand delivery .	51
3.3.1	Landslide locations, volumes, and grainsize	51
3.3.2	Landslide sediment entrainment into the river	53
3.3.3	Effects of landslide dams.....	53
3.3.4	Sediment transfer to the coast.....	54
3.3.5	Landslide sand transfer along the coast.....	57
3.4	Effects of future sand budget changes on sand volumes and shoreline position..	57
3.4.1	Summary of potential sand budget changes.....	57
3.4.2	Effects on beach budget and shoreline position trends	59
3.5	Effects on Waimakariri River mouth stability.....	63
3.6	Effects on inundation.....	63
4	Conclusions	65
5	Acknowledgements	67
6	Glossary of acronyms	68
7	References.....	69
Appendix A	Kidson Weather Types	72
Appendix B	WASP wind scaling	73

Tables

Table 2-1:	Climate change scenarios used for simulating future Waimakariri River flows and suspended load.	15
Table 2-2:	Climate change and sea-level scenarios used with SWAN modelling.	21
Table 2-3:	Input data for the morphodynamic model of the lower Waimakariri River.	25
Table 3-1:	GCM-averaged long-term average suspended load by climate change scenario, and time-trend statistics.	32

Table 3-2:	Means and maxima of TopNet-modelled Waimakariri at Otarama flows for 2008-2016 for the six GCM realisations of the RCP2.6 and RCP4.5 climate change scenario, compared with mean and maximum.	33
Table 3-3:	Commentary on changes (from Baseline) in wave energy and longshore transport patterns under climate-change and sea-level rise scenarios.	44
Table 3-4:	Inner and outer profile closure depth estimates at Southshore, Parklands, and Pines Beach wave output stations for climate change and sea-level rise scenarios.	48
Table 3-5:	Avon-Heathcote Estuary Ihutai spring-tide tidal-prism volume and throat cross-section area.	49
Table 3-6:	Estimated ebb-delta and inlet throat sand volume changes after Christchurch Earthquake and sea-level rise.	50
Table 3-7:	Location and size of six indicative major earthquake induced landslides in the Waimakariri Catchment.	52
Table 3-8:	Estimated landslide dam lake volumes and fill times.	53
Table 3-9:	Impacts of future sand budget scenarios on alongshore-averaged shoreline shift rate, Waimakariri to Sumner.	62
Table B-1:	Wind climate parameters from the WASP simulations.	73

Figures

Figure 1-1:	Current sand budget for Southern Pegasus Bay shore.	11
Figure 2-1:	Normalised suspended sediment rating curves for Waimakariri, Rakaia, and Rangitata Rivers.	14
Figure 2-2:	Workflow for “futurecasting” nearshore wave records in Pegasus Bay from GCM output.	19
Figure 2-3:	Time-averaged directional spectra near the Banks Peninsula wave buoy from the WASP baseline and changes to this for Scenario B2 and Scenario A2 simulations.	20
Figure 2-4:	Annual mean wave energy spectra from the Banks Peninsula wave buoy (coloured lines), compared to the 30-year (1970-2000) average spectrum from the WASP baseline simulation (black line).	21
Figure 2-5:	Lower Waimakariri River morphodynamic model extent.	24
Figure 2-6:	Schematic of shore budgeting model.	27
Figure 2-7:	Budget of sand distribution from the Waimakariri River mouth.	27
Figure 2-8:	Offshore profile surveys at Beatty Street and Spencer Park.	29
Figure 2-9:	Beatty Street and Spencer park profiles distance-offshore scale transformed to the power of 2/3.	29
Figure 3-1:	Projected future Waimakariri suspended loads from TopNet modelling with climate change scenarios.	31
Figure 3-2:	TopNet-modelled hydrographs of Waimakariri at Otarama flows for 2008-2016 for three GCM realisations of the RCP2.6 climate change scenario, compared with observed flows.	33
Figure 3-3:	Flow-distribution curves at Waimakariri at Otarama for period 2008-2016 for TopNet-modelled outputs of GCMs for (a) RCP2.6 and (b) RCP8.5 climate change scenarios, compared with observed flow duration curve.	34

Figure 3-4:	Proportions of catchment area, runoff, and suspended sediment load associated with the upper (above gorge), middle (gorge and front-ranges), and lower (Canterbury Plains) parts of the Waimakariri Catchment.	35
Figure 3-5:	Projected % changes in average annual rainfall by 2090 under the RCP2.6 (low emissions) and RCP8.5 (high emissions) climate change scenarios, relative to 1995 baseline.	36
Figure 3-6:	Late-century % changes (median across multiple GCMs) in mean annual flood for RCP2.6 (low emissions) and RCP8.5 (high emissions) climate change scenarios.	37
Figure 3-7:	Wave energy and longshore transport potential along Pegasus Bay under different climate change and sea-level rise scenarios.	43
Figure 3-8:	Avon-Heathcote Estuary ebb-delta bathymetry.	49
Figure 3-9:	Location of six indicative potential major landslides in Waimakariri Catchment.	51
Figure 3-10:	Google Earth images of indicative major landslides.	52
Figure 3-11:	Landslide grainsize distribution selected for modelling compared to measured grainsize distributions of a number of landslide deposits.	54
Figure 3-12:	Estimated rate of delivery of all sediment and sand into the Waimakariri River system from earthquake induced landslides.	55
Figure 3-13:	Modelled coastal sand delivery with and without earthquake induced landslide activity.	56

Executive summary

Background

The Christchurch City Council Land Drainage Recovery Programme (LDRP) seeks to understand the post Canterbury Earthquake Sequence flood risk in the Greater Christchurch area by considering the influence of co-location, coincidence, and cascading of multi-hazards. Coastal erosion and inundation are two such hazards that link to other hazards, with their severity potentially affected by direct and indirect effects of earthquakes (e.g., shore uplift/subsidence, tsunami, landslide contributions to river sand delivery) and by rising sea-level and changing wave-climate.

Accordingly, Christchurch City Council commissioned a study to provide updated information on the current coastal sediment budget (Stage A) as well as better understanding of how future changes in this budget may affect coastal erosion and inundation extents (Stage B), which in turn may influence floodplain and land-use management. The Stage A results were reported recently in Hicks et al. (2018). This report presents the results from Stage B, focussing on potential changes in the future coastal sediment budget and their consequences.

Objectives

The Stage B study objectives were to assess potential changes in the coastal budget due to climate change effects (including changes in the Waimakariri River flow, wave climate, and sea-level rise) and a large earthquake affecting the Waimakariri catchment, and to assess the impact that any projected changes in the coastal sediment budget would have on future shorelines, river mouth stability, and inundation hazards.

Methods

Two potential effects of climate change on the Waimakariri River's supply of beach-grade sand were considered. Firstly, changes in the hydrological drivers that directly influence catchment erosion and sediment transfer were inferred from regional climate change assessments and guidance, predictions of changes in the frequencies of Kidson Weather Types over Canterbury, and analysing results from numerical simulations of future Waimakariri River flows under a range of climate change scenarios. Secondly, indirect effects of human responses to climate change were considered, including land use change effects on erosion and "collateral" sand loss from the river associated with increased irrigation water takes and gravel extraction.

Increased sand delivery to the coast stemming from landslides in the Waimakariri Catchment associated with a large alpine earthquake was simulated using a one-dimensional numerical sediment routing model.

Changes to the wave climate at the Christchurch City shore due to global climate change and sea-level rise were assessed by using the SWAN model to transform climate-change-altered deep-water wave climates into Pegasus Bay assuming the existing sea-level and a sea-level 1.36 m higher. The SWAN model results were used to quantify the impact on longshore sand transport and beach profile closure depth.

The effects of future changes to various components of the coastal sand budget on beach volumes and shoreline position were assessed using a spreadsheet-based sediment budgeting model.

Findings

The Waimakariri River's future sand delivery to the tidal reach due to climate change effects and human responses could vary between an estimated reduction of 11% (8% reduction from up-

catchment and 3% interception by irrigation takes) and a 28% increase (28% increase from up-catchment and all irrigation-intercepted sand flushed back to the river). The mid-range of these estimates is for a net load increase of 9%. Sea-level rise driven deposition in the tidal reach of the Waimakariri River would reduce the river sand delivery to the coast by 1% or less.

Following a major future alpine earthquake, landslides (300 million m³ combined volume of which 20% renders to sand) clustering mainly in or just upstream of the Waimakariri Gorge could double (possibly treble) the river's sand load for over 10 years, with landslide sand first arriving at the coast within 1-2 years of the landslide event, and 90% of the landslides' coastal sand delivery occurring over 30 years. Dispersion of the landslide's sand pulse along the shore by coastal processes would likely occur slowly, with several decades elapsing before any signature appeared at Waimairi Beach and longer to reach Southshore. Although there are significant uncertainties with what sand volumes might actually be discharged after any particular earthquake, the time-scales of the sand transfers are considered more reliable.

Under sea-level rise and a climate-change-altered nearshore wave climate, the proportion of river sand load transported south from the Waimakariri River mouth could change from the baseline estimate of 68%. Both the A2 (aligning with the IPCC5 RCP8.5 "high emissions" greenhouse gas concentration trajectory) and B2 (aligning with the IPCC5 RCP6.0 "higher emissions but stabilising" trajectory) wave scenarios would reduce the proportion of Waimakariri River sand transported south by virtue of relatively reduced wave energy from the northeast quarter. A rise in sea level with no change in offshore wave climate would increase the proportion of sand load transported south. While combinations of sea-level rise and wave climate change would have compensating effects, the wave climate change would prevail, resulting in reduced proportions transported south.

Beach profile closure depth would increase with sea-level rise (due to more wave energy incident on the shore), decrease under the A2 and B2 wave scenarios (due to reduced storm wave energy), but not change much under combined sea-level rise and wave climate change scenarios. An increased closure depth increases the sand volume required to lift the beach profile to match a rise in sea-level.

The net sand demand for enlarging the Avon-Heathcote Inlet ebb-delta and throat associated with rising sea-level could be anywhere between zero and 8% of the present river sand supply rate to the City shore.

The sediment budget model showed that at least until 2120, the City shore sand budget should remain in surplus (and the shore should not begin to erode) except under the worst case RCP8.5 climate change scenario (which couples the effects of changed Waimakariri River sand load, sand losses due to future irrigation takes, reduced southward wave-driven sand distribution from the river mouth, a 1.36 m sea-level rise, and sand losses to the ebb-delta at the Avon-Heathcote Inlet). We caution that this is a spatially-averaged result, and actual shoreline movements are likely to vary locally from the average rate. Numerical shore modelling would be required to develop spatially-detailed shore responses.

A significant future shore instability at the Waimakariri River mouth would likely accompany the arrival of a sand pulse following earthquake-triggered landslides in the upper Waimakariri Catchment. The river delta would enlarge, sand bars would become larger and more active, interactions between bars and the shoreline would increase in amplitude, and possibly another spit and foredune system could form seaward of the present one. Otherwise, the recently-observed cycles of spit-tip erosion and bar changes should continue into the future. The risk of waves over-

washing Brooklands Spit and the Waimakariri River suddenly re-locating its outlet through Brooklands Lagoon is small, even under wave climate change and sea-level rise scenarios.

Key conclusions

At least up to 2120, the City shore sand budget should remain in surplus, and the shore should not begin to erode, except under the worst case RCP8.5 climate change scenario. Unless that scenario eventuates, we do not anticipate the risk of sea-flooding from the ocean-side will generally be exacerbated by shore erosion and sea-level rise. The exception will be at the southern tip of Southshore Spit due to the Avon-Heathcote Inlet widening as sea-level rises and the tidal prism increases.

1 Introduction

1.1 Background and objectives

The Christchurch City Council (Council) Land Drainage Recovery Programme (LDRP) seeks to understand the post Canterbury Earthquake Sequence flood risk in the Greater Christchurch area by considering the influence of co-location, coincidence, and cascading of multi-hazards. Coastal erosion and inundation are two such hazards that link to other hazards, with their severity potentially affected by direct and indirect effects of earthquakes (e.g., shore uplift/subsidence, tsunami, landslide contributions to river sand delivery) and by rising sea-level and changing wave-climate.

The coastal sediment budget is a key control on coastal erosion and inundation, but, as detailed in the LDRP113 Coastal Sediment Budget Study (Council 2017), there are knowledge gaps, or at least significant uncertainties, in components of the contemporary budget as well as how it might change in the future.

Accordingly, Council commissioned a study to provide updated information on the current coastal sediment budget as well as better understanding of how future changes in this budget may affect coastal erosion and inundation extents, which in turn may influence floodplain and land-use management. The study results are to be fed into the multi-hazard analysis of the wider LDRP97 Project in preparing floodplain management plans. It is also anticipated that the project outputs will be used by Council's Land Drainage Team and Strategic Policy Unit in the course of long term and regeneration planning.

The study has been split into two stages:

- Stage A – updated sediment budget.
- Stage B – assessment of future sediment budget effects.

The objective of Stage A was to update the contemporary coastal sediment budget for the Christchurch beaches, including updating the supply of beach sand from the Waimakariri River, the longshore transport potential of waves incident on the Christchurch shore, and the sand volume stored in the beaches. The Stage A results are reported in Hicks et al. (2018) and summarised below.

The Stage B objectives are to assess potential changes in the coastal sediment budget due to climate change effects (including changes in the Waimakariri River flow, the wave climate, and sea-level rise) and a large earthquake affecting the Waimakariri catchment, and to assess the impact that any current or projected future changes in the coastal sediment budget would have on future shorelines, river mouth stability, and inundation hazards.

This report presents the results from Stage B, focussing on potential changes in the future coastal sediment budget and their consequences.

1.2 Summary of current sand budget

The contemporary coastal sand budget, developed in Stage A and representing the past several decades, provides the baseline from which to assess future changes. The components of this current budget (from Hicks et al. 2018) are summarised in Figure 1-1.

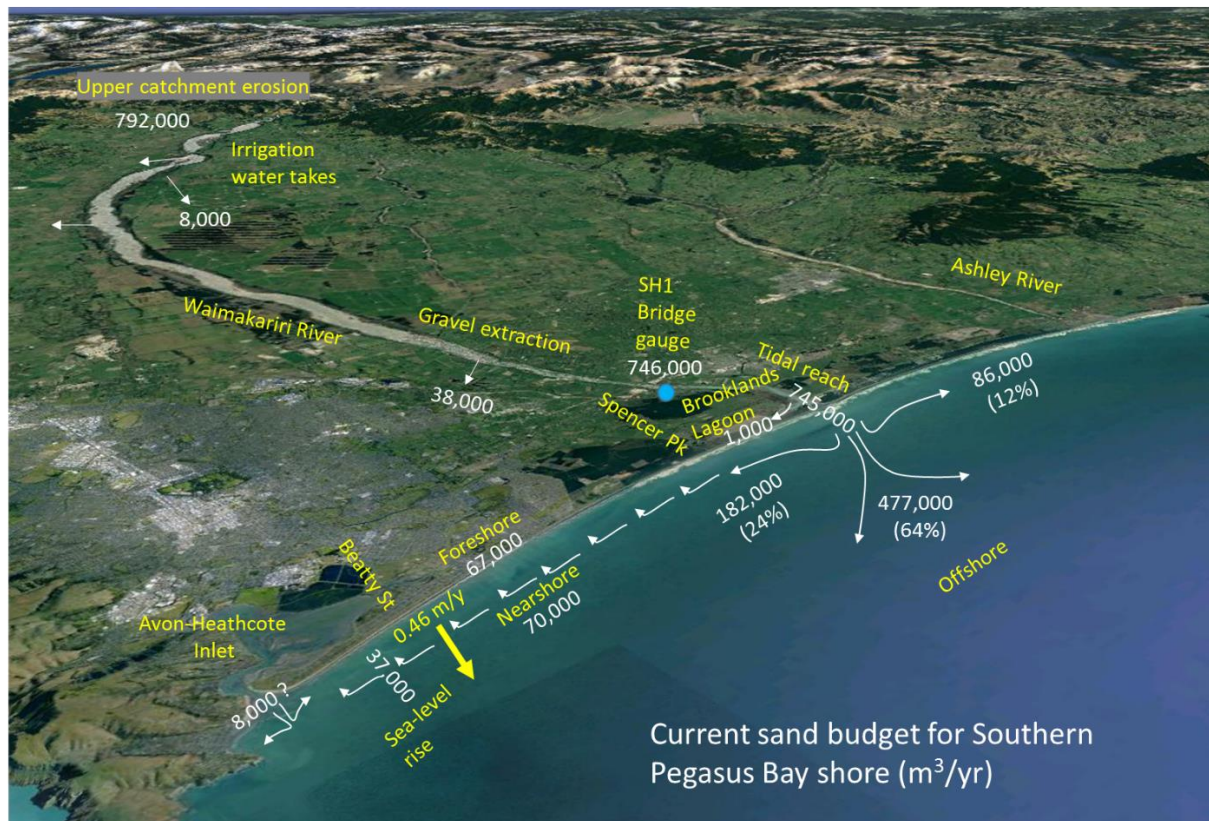


Figure 1-1: Current sand budget for Southern Pegasus Bay shore. Yellow figures show the space-time-averaged rate of shoreline advance between the Waimakariri River mouth and Sumner. The Waimakariri River's sand load is measured at the flow-recording gauge at the SH1 bridge (blue dot). Small components of the river's sand load are lost between the mountains and the sea to irrigation takes, gravel extraction, and deposition in Brooklands Lagoon. Only a fraction (68% of 36% = 24%) of the river's sand is distributed to the beaches southward from the river mouth, but this has been enough to prograde the shoreline while lifting the profile to match rising sea-level. A one-off sand supply to the adjacent beaches from the Avon-Heathcote inlet's ebb-tidal may have occurred following the Christchurch Earthquake sequence but its quantity is very uncertain.

Key points are:

- The dominant sand source is the Waimakariri River ($746,000 \text{ m}^3/\text{yr}$ measured at the flow-recording gauge at the SH1 bridge). Although small components of the river's sand load are lost between the mountains and SH1 to irrigation takes and gravel extraction, these losses are accounted for in the load measured at SH1. Between SH1 and the coast, there is also a very small sand loss ($1,000 \text{ m}^3/\text{yr}$) to deposition in Brooklands Lagoon.
- At the river mouth, 64% of the river sand load, comprising the finest sand fractions that are not found in the beach material, are dispersed offshore. Of the residual 36%,

comprising the coarser sand fractions, 68% (182,000 m³/yr) is transported southward towards the city shore and 32% (86,000 m³/yr) is transported northward. The southward transport is driven by northeast waves which prevail over southerly swell along the southern part of Pegasus Bay. The southerly swell progressively dominates and causes a net northward longshore transport along the northern part of Pegasus Bay.

- The sand transported south of the river mouth has resulted in an overall-average progradational trend (i.e., shoreline advance) of 0.46 m/yr along that shore. Of the total southwards-directed river sand supply of 182,000 m³/yr: progradation of the foreshore (above mean sea level) has consumed 67,000 m³/yr; progradation of the nearshore segment of the beach profile (above the profile 'closure depth') has consumed 70,000 m³/yr; while lifting both foreshore and nearshore segments of the profile to match an historical sea-level rise of 2 mm/yr has required 37,000 m³/yr of sand.
- This leaves a small sand budget misclose of 8,000 m³/yr. This misclose increases to 16,000 m³/yr if an additional (but very uncertain) one-off sand supply event from the Avon-Heathcote ebb-tidal delta following the Christchurch Earthquake Sequence (equating to 8,000 m³/yr when averaged over the budgeting time-frame) is considered. These small miscloses are well within the uncertainty of the major sand budget components – notably the river sand load and the proportions of that which are lost offshore and moved south from the river mouth.

2 Methods

In overview, the Stage B workflow comprised four main tasks:

- Assessing the effect of climate change on the Waimakariri River's supply of beach-grade sand, including hydrological effects and human responses.
- Assessing changes to the wave climate at the Christchurch City shore due to global climate change and sea-level rise, and the impact on longshore sand transport and beach profile closure depth.
- Assessing changes to the Waimakariri sand delivery associated with an Alpine Fault earthquake.
- Assessing the effects of future sand budget changes on beach volumes, shoreline position, river mouth and inlet stability, and inundation.

In the following sub-sections, we outline the methodologies associated with these tasks and discuss some of their limitations. Uncertainties and limitations are further addressed with the results in Section 3.

2.1 Climate change effects on Waimakariri River supply of beach-grade sand

Changes in the Waimakariri River's sand load associated with climate change could be due directly to hydrological changes in the catchment, which could alter erosion rates and sediment delivery from the catchment, and indirectly through human responses to climate change – for example, extracting more irrigation water with sand extracted at the same time. Sea-level rise is also expected to promote some sand deposition in the tidal reach of the Waimakariri River.

2.1.1 Waimakariri sand load change associated with hydrological change

Underpinning assumptions

Our assessment approach is underpinned by two assumptions:

1. That the ratio of the Waimakariri River's sand load to its suspended load will remain unchanged with future climate change. This is based (i) on the results from Hicks et al. (2018) that the Waimakariri sand load is carried dominantly as suspended load, and (ii) on the broader appreciation that the suspended load's size grading is related mainly to catchment lithology (Hicks et al. 2018), which will not change.
2. That the Waimakariri River's suspended sediment load is related to its water discharge, and this relationship is unlikely to change much while the climate changes. The Waimakariri suspended sediment rating curve developed by Hicks et al. (2018) explains 96% of the variance in the observed suspended load, and so demonstrates this high correlation. We assume that this rating will not change substantially because we expect that any changes in catchment rainfall will produce proportional changes in both runoff and sediment delivery. Validation of this comes from overlaying the sediment rating curve from the Waimakariri with those from the Rangitata and Rakaia Rivers after normalising discharge by the mean discharge – which results in the data from all three rivers plotting in the same "space" (Figure 2-1).

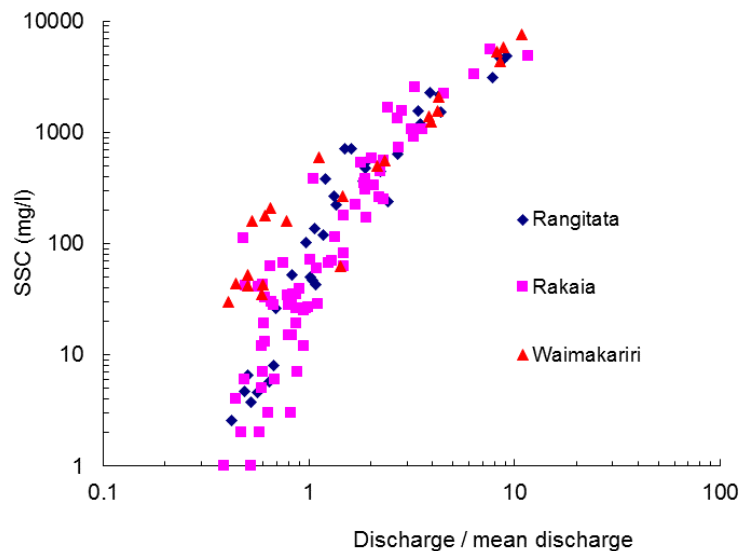


Figure 2-1: Normalised suspended sediment rating curves for Waimakariri, Rakaia, and Rangitata Rivers. Discharge has been normalised by dividing by the mean discharge.

With these assumptions, we explored how the Waimakariri's suspended load might change due to climate-change-driven hydrological change using three approaches:

1. Examining regional projections on flow regime change from national guidance documents.
3. Estimating future suspended sediment loads using a linked climate-hydrological modelling approach coupled with the suspended sediment rating curve.
4. Interpreting the consequences of projected change in Kidson Weather Types.

[Regional projections of flow regime change](#)

This drew on national guidance documents (MfE 2016a, MfE 2016b, Collins and Zammit 2016) that included projections of hydrological and flow regime change in Canterbury. Typically, these documents include advice on changes in mean flow, extreme flows, and seasonality.

[Linked climate-hydrological modelling approach coupled with the sediment rating curve](#)

This approach involved combining the river's suspended sediment rating curve with flow records simulated for various climate change scenarios to directly calculate future suspended loads in the Waimakariri River out to 2100. For this we utilised flow records that were already simulated using NIWA's TopNet hydrological model (C. Zammit, NIWA, pers. comm.). The key elements of these simulations are:

- Hourly flow records were generated by the TopNet model at the Otarama flow gauge site¹ (at the lower end of the Waimakariri Gorge) for the period 2006 through 2100.
- The TopNet model was run with output from 24 runs of a Regional Climate Model (RCM), each driven by six Global Climate Models (GCMs) simulating four different climate change scenarios as represented by four Representative (greenhouse gas) Concentration Pathways (RCPs).
- The TopNet model for the Waimakariri at Otarama was calibrated from observed flows and climate data (Zammit and Woods 2011).

The RCPs are defined fully in the IPCC5 report (IPCC 2014); the essential differences among the RCPs reflect how the global community responds by altering greenhouse gas emissions (Table 2-1). The six² GCMs were chosen (from a much larger suite of GCMs available internationally) by Mullan et al. (2016) on the basis that they do a reasonably good job of hindcasting New Zealand weather. The RCM, which downscales the GCM results onto a finer grid covering New Zealand, was developed and run by NIWA (Mullan et al. 2016). These downscaled RCP realisations with the same six GCMs have been the basis of several national and regional projections of future climate and hydrology (e.g., Mullans et al. 2016, Collins and Zammit 2016, MfE 2016a, MfE 2016b, Smart et al. 2018).

We combined the simulated future flow records with the existing suspended sediment rating curve to generate estimates of annual suspended load between 2006 and 2100.

We checked how well the simulated flows for the period 2008-2016 compared against the observed flows at Otarama in regard to the mean and maximum flow and the flow-duration curve (which exerts dominant control on the sediment load).

Table 2-1: Climate change scenarios used for simulating future Waimakariri River flows and suspended load. The scenarios relate to Representative Concentration Pathways (RCPs) of greenhouse gases, based on a range of human responses to the climate change issue. The RCPs are detailed in IPCC (2014).

Scenario	Greenhouse gas emissions trend
RCP2.6	Peaking then declining
RCP4.5	Stabilising
RCP6.0	Stabilising but at a higher level
RCP8.5	Continuing to rise

¹ Comparison of the mean flows for the period 30/5/2008 to 3/6/2016 at Otarama (113.7 m³/s) and the Old Highway Bridge (OHB) gauge near the coast (114.6 m³/s) showed minimal difference, so we made no adjustment to convert Otarama flows to flows at OHB, which is where the sediment rating curve has been established.

² Many international institutions have developed GCMs, which can be used for hindcasting, forecasting, or projecting future weather across the Earth. These models all differ in detail, and it is likely that some deal better than others with some aspects of atmospheric physics (and vice-versa), so even though they might all be set up to simulate the same future emissions scenario (i.e., RCP), they will all produce somewhat different results. It has become convention with climate change modelling to not rely on any single GCM result but to look at the range of results from multiple models, with the expectation that the true result will lie within the bounds of the set of modelled results, most-likely around their mid-range.

Changes in Kidson Weather Types

Kidson (2000) developed a classification of 12 synoptic weather types that characterise recurring atmospheric circulation patterns over New Zealand, as observed on weather maps (Appendix A). Changes in the frequency-of-occurrence of these over Canterbury due to future climate change were assessed by Smart et al. (2018), as part of the wider LDRP97 Project for Council. In this report we assess how these changes in Kidson Weather Types might impact erosion rates in the Waimakariri Catchment, and hence the river's sand load.

2.1.2 Human response effects

To consider the effects of human response to climate change on the river sand yield we considered two possible effects:

- changes in gravel extraction rates, and
- changes in sand diversion with irrigation water take extraction.

Assessing effects due to changed gravel extraction rates drew on discussion developed in the Stage A report (Hicks et al. 2018).

The amount of sand removed from the river via water abstraction was estimated as equivalent to 1.1% of the river's sand discharge to the coast in the Stage A report. To estimate potential changes in sand removal due to changes in the future water abstraction regime we reviewed relevant strategic planning documents to develop a simple scenario representing the maximum probable future abstraction. Based on this scenario, we estimated "collateral" sand removal using the same approach as was used for the current abstraction regime in the Stage A report. These calculations were based on the current flow regime and assumed that the sediment rating curve and sand proportion of the suspended load remains unchanged.

2.1.3 Sand entrapment in the tidal reach of the Waimakariri River and Brooklands Lagoon

Hicks et al. (2018) assumed that bed levels along the sand-bedded tidal reach of the Waimakariri River are currently stable (on an annual average basis) and are in equilibrium with the river flow, sand supply from upstream, and tide levels. For this study, we assumed a similar equilibrium would be maintained under a higher sea-level, which would require sand deposition in the tidal reach to lift the bed to match the sea-level rise, which in turn would reduce the sand delivery to the coast. This sand deposition rate was calculated as the product of the tidal reach surface area and the rate of sea-level rise.

We have assumed no additional sand interception by Brookland's Lagoon under higher sea-levels, as Hicks et al. (2018) concluded that the lagoon is currently accumulating mainly mud grade sediment and very little sand.

2.2 Effects of wave climate change and sea-level rise

2.2.1 Overview

Climate change could influence the nearshore wave climate along the City shore in two ways: (i) by altering the deep-water wave climate, and (ii) by altering wave refraction and shoaling due to increased water depths associated with sea-level rise. Consequent changes in the nearshore wave climate could alter the longshore transport regime. For example, an intensification of southerly-sourced wave energy could change the present balance between northward and southward

transport from the Waimakariri River mouth, reducing the share of the Waimakariri sand yield that is delivered to the City's beaches and 'flipping' the city shore into an erosion trend. A changed nearshore wave climate could also change the profile closure depth, which would then change the demand for sand to sustain the profile against rising sea-levels, also potentially promoting erosion. Rising sea-level could also increase the tidal prism volume of the Avon-Heathcote Estuary, creating a demand for sand from the adjacent beaches to stock enlarged tidal deltas.

The workflow to examine these climate change effects on coastal processes was as follows:

- Reviewing national guidance documents on future changes in wave climate.
- Building on other work to derive simulated future deep-water wave records at the Banks Peninsula wave site, and transforming these onto the City shore using the SWAN model, including repeat runs with a sea-level 1.36 m higher (see below for further information on sea-level scenarios).
- Analysing the transformed wave records for differences in longshore transport potential and closure depth relative to the baseline condition, which is the SWAN-transformed measured 2000-2017 wave record.
- Assessing changes to the Avon-Heathcote Estuary tidal prism associated with sea-level rise and the consequent effects on the ebb tidal delta size.

2.2.2 Future sea-level

We ran the SWAN model with two sea-level scenarios: the current (baseline) sea-level, and a sea-level rise of 1.36 m, which aligns with the upper bound estimate by 2120 used by Tonkin & Taylor (2017) in their assessment of future shoreline positions³. To avoid simulating many sea-level and wave scenario combinations with the SWAN model (which would have required several more weeks of supercomputer CPU time), we assumed that the effects of intermediate sea-level rises (e.g., 0.55 m) could be estimated by linear interpolation of the results for the baseline and 1.36 m cases.

2.2.3 Changes to the wave climate

National Guidance

National guidance on what to plan for around future wave climate at the New Zealand coast remains fairly 'broad brush'. For example, MfE (2008) recommended for the eastern South Island coast north of Banks Peninsula, for the period 2050-2100:

- Assume a 10% increase in the extreme deep-water wave climate (above 1% Annual Exceedance Probability significant wave height).
- For nearshore wave modelling, assume a 10% increase in the frequency of winds from the westerly sector (but not necessarily changes in wind speed).

Most recently, MfE (2017) suggested assuming a 0-10% increase in the heights of large (99% percentile) waves out to 2100. This was based on futurecasts undertaken for the Wave and Storm-Surge Projections (WASP) project (Gorman and Bell 2011, Gorman 2016).

³ Tonkin & Taylor (2017) considered possible sea-level rises out to 2065 and 2120 under four climate change scenarios. This provided sea-level rises ranging from 0.3 m to 0.55 m by 2065 and from 0.55 to 1.36 m by 2120.

Predictions made for this study

Since the City shore is sensitive to the balance between southerly and north-easterly sourced waves (which is not informed by the MfE guidance), for this study we made use of the *WASP* projections undertaken by Gorman (2016) to generate deep-water wave records at the Banks Peninsula wave-buoy for a range of future climate change scenarios. The key elements of this approach (summarised in Figure 2-2) involved:

- Using output from Global Circulation Models (GCMs) coupled with Regional Circulation Models (RCMs) to force nested global and regional implementations of the Wavewatch III model.
- The coupled simulations were associated with a 30-year (1970-2000) baseline period and with four future emissions scenarios (three variants of Scenario A2 and one of Scenario B2) for the 2070-2100 period that were chosen from the AR4 SRES emissions scenarios (IPCC 2000). The A2 scenario represents a more “divided world”, with population continuing to increase and a focus on regional economic development. It is on the high side for continuing increase in CO₂ emissions, and aligns reasonably with the RCP8.5 scenario (Table 2-1). The three A2 scenarios (referred to as A21, A22, A23) differed only due to their initial conditions, and we worked with averaged results from these. The B2 scenario is also a “divided world” but with a stronger focus on environmental rather than economic issues. While CO₂ emissions still increase under the B2 scenario they do so at a much slower rate than in the A2 scenario and thus represent one of the lower scenarios in the AR4 SRES suite. The B2 scenario aligns reasonably with the RCP6.0 scenario (Table 2-1).
- The outputs from the wave model simulations for the 30-year baseline hindcast and for each of the 2070-2100 futurecasts included 30-year records of full directional wave spectra $S(f, \theta, t)$ at selected grid cells. For this study, we selected the offshore cell of the regional grid that was closest to the Banks Peninsula wave buoy site: this is located at 44.3750°S, 173.4375°E. The wind fields from the corresponding RCM simulations at this cell were also extracted.
- The 30-year time-average of the wave spectra, $\langle S(f, \theta) \rangle$, at this site, taken for the baseline simulation and for each futurecast, were then used to provide a frequency- and direction-dependent spectral scaling factor:
$$A(f, \theta) = \langle S(f, \theta) \rangle_{proj} / \langle S(f, \theta) \rangle_{base} \quad (1)$$
- This scaling factor was then applied (after interpolation to different discrete frequency and direction bins) to the actual measured wave buoy spectra record to generate equivalent wave buoy records associated with the various futurecasts. In the case of the A2 scenarios, a scaling factor averaged over the three realisations (A21, A22 and A23) was used.
- Wind inputs for the SWAN model were also modified to align with the future scenarios using a similar scaling approach, as detailed in Appendix B.
- The “future adjusted” wave buoy and wind records were then transformed to nearshore waves using the SWAN model, either assuming present sea-level or assuming a sea-level rise of 1.36 m.

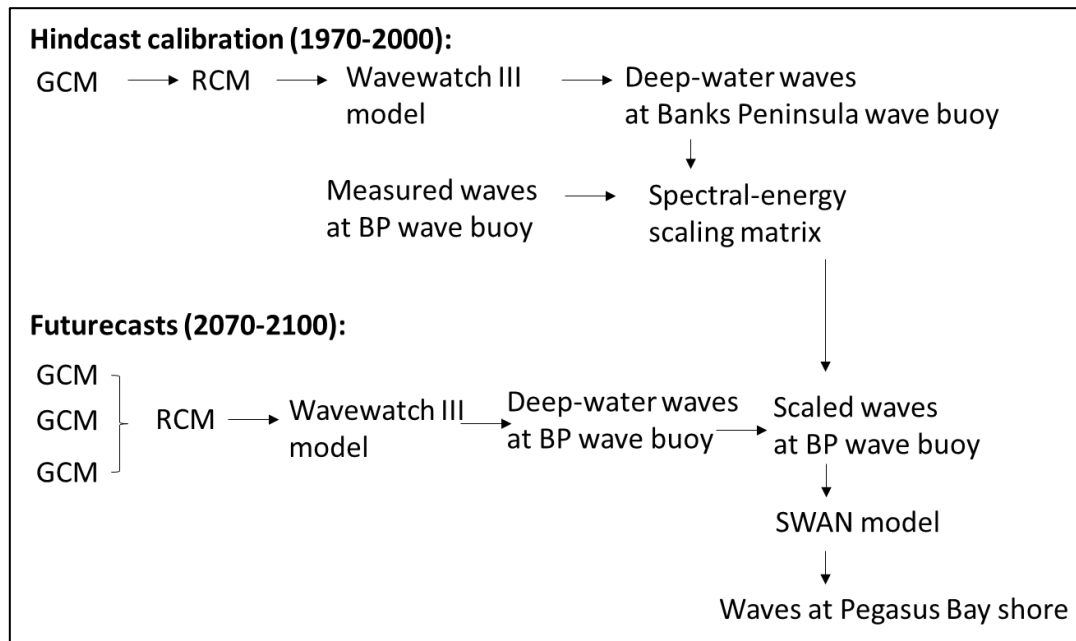


Figure 2-2: Workflow for “futurecasting” nearshore wave records in Pegasus Bay from GCM output. Key component is a spectral scaling matrix, calibrated off hindcast data, which converts the measured Banks Peninsula (BP) wave record (across the wave-frequency and direction domains) into equivalent records under future climate change scenarios. These records are then refracted into Pegasus Bay using the SWAN model.

This approach will capture a mean shift in wave climate between the baseline (i.e., as measured) and the given futurecast. That is, it will rescale the mean energy associated with waves of each frequency and propagation direction. The spectral scaling factors $A(f, \theta)$ obtained in this way are plotted in Figure 2-3, overlaid with contour plots of the mean baseline spectrum $\langle S(f, \theta) \rangle_{base}$. The mean spectrum is dominated by a primary swell peak from the SSW (Cartesian direction $\sim 60^\circ$), with secondary peaks from the ENE and ESE. In the case of the A2 scenario (Figure 2-3, top panel), for example, energy in the SSW swell peak is generally scaled up, while energy from the easterly sector is generally reduced. For the B2 scenario (Figure 2-3, lower panel) there is more variability in the patterns of energy change across the main spectral peaks.

One potential limitation of this approach is that wave direction and frequency bands which only rarely contain energy in either the baseline or climate change projection simulations will tend to produce particularly high or low scaling factors, respectively. This may excessively modify the buoy-derived spectra in these bands, which could be a problem if such bands are more prominently represented in the buoy record than in the WASP simulations. However, we see from Figure 2-4, comparing averaged energy spectra from the buoy and the WASP baseline, that at least in frequency space there is consistent agreement in the shape of the spectrum, i.e., where energy is located, even though the magnitude of the buoy spectrum shows considerable inter-annual variability. Thus, we consider the risk is low that this potential effect has produced misleading results.

Another limitation is that more detailed changes in wave climate may not be captured by this approach. For example, a change in the temporal clustering of storms, or a shift to fewer “moderate” storm events but more “extreme” storms, may not affect the mean spectra.

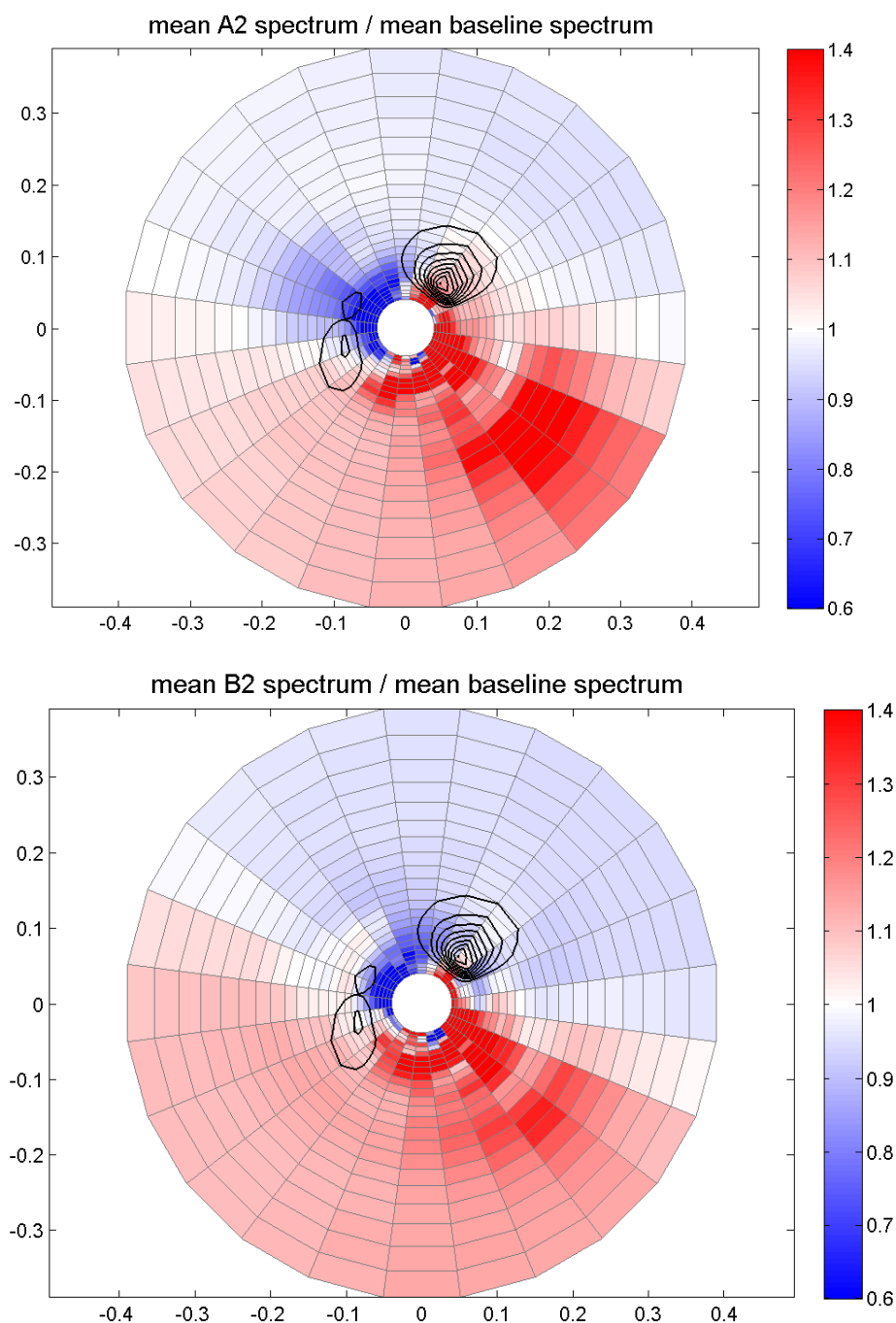


Figure 2-3: Time-averaged directional spectra near the Banks Peninsula wave buoy from the WASP baseline and changes to this for Scenario B2 and Scenario A2 simulations. The black contours in both panels show the mean spectral density for the baseline simulation. The coloured grid-squares indicate the ratio of wave energy density per directional and frequency band in the A2 (top panel) and B2 (bottom panel) simulations to the energy density in the baseline simulation. The polar plots show directions towards which waves travel (north at top, east at right), while both horizontal and vertical axes show wave frequency (waves per second) in each quadrant. For example, the major source of baseline wave energy, arriving from the SSW, appears in the upper right quadrant and its peak energy occurs at a frequency of approximately 0.07 (equivalent to a period of 14 seconds).

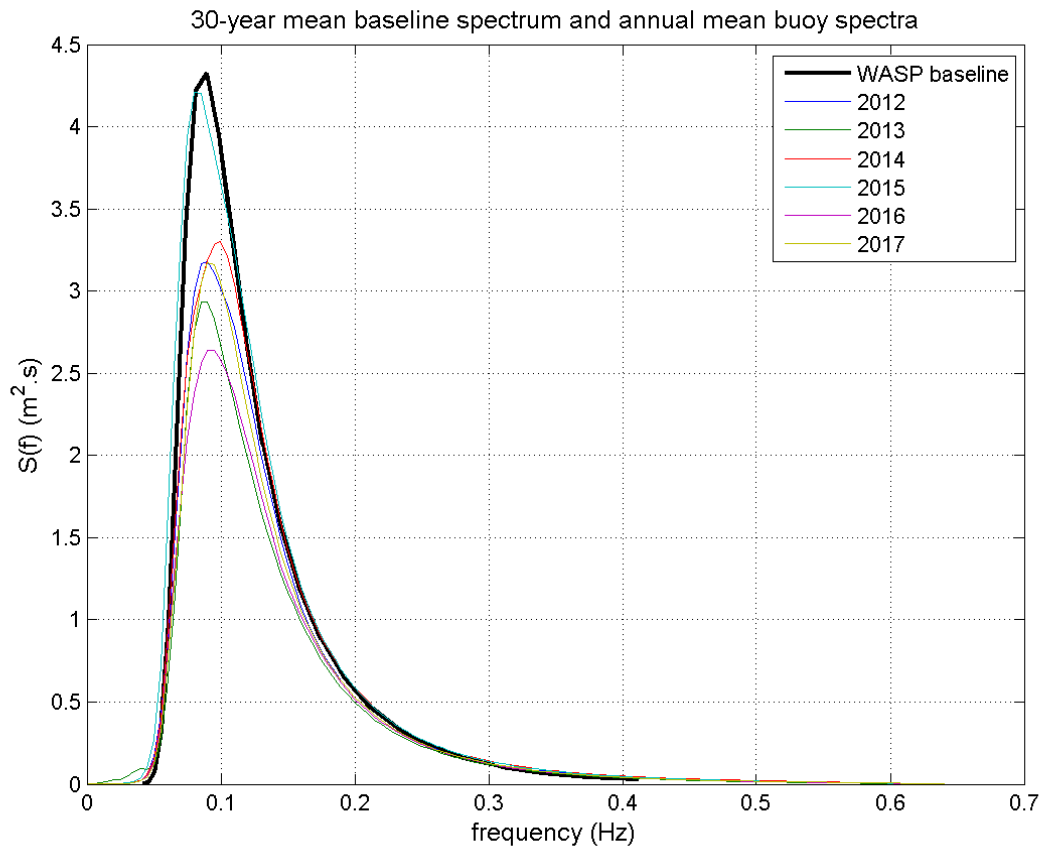


Figure 2-4: Annual mean wave energy spectra from the Banks Peninsula wave buoy (coloured lines), compared to the 30-year (1970-2000) average spectrum from the WASP baseline simulation (black line).

2.2.4 SWAN modelling scenarios

We thus compared SWAN model output from six scenarios, each with a different combination of climate change and sea-level rise scenarios, as listed in Table 2-2.

Table 2-2: Climate change and sea-level scenarios used with SWAN modelling. Note that Scenario A2 aligns reasonably with Scenario RCP8.5 in Table 2-1, while Scenario B2 aligns with Scenario RCP6.0 in Table 2-1.

SWAN Scenario	Climate change scenario	Sea-level scenario
Baseline	Existing	Existing
SLR	Existing	+ 1.36 m
A2	A2 (~ RCP8.5)	Existing
A2+SLR	A2 (~ RCP8.5)	+ 1.36 m
B2	B2 (~ RCP6.0)	Existing
B2+SLR	B2 (~ RCP6.0)	+ 1.36 m

2.2.5 Changes in longshore transport potential and beach-profile closure depth

We assessed longshore transport potential from the SWAN model output for the various nearshore wave scenarios as detailed in Sections 2.2.1 and 2.2.2 of Hicks et al. (2018). We assessed the inner and outer closure depth limits from the SWAN model output using the Hallermeier relations as detailed in Section 2.3.2 of Hicks et al. (2018).

2.2.6 Avon-Heathcote Estuary tidal prism and sand entrapment

Changing sea-levels are likely to affect the tidal prism of the Avon-Heathcote Estuary / Ihutai, with the “knock-on” effect of changing the volume of sand stored in the estuary ebb tidal delta. Hicks and Hume (1996) investigated the relationship between estuary spring-tide tidal-prism volume and the volume of sand stored in ebb tidal deltas for 17 New Zealand estuaries. They found that 83% of the variance in ebb delta volume was explained by the function:

$$V = 0.000188 \Omega^{1.41} \quad (2)$$

Where V is the ebb-tidal delta bulk sand volume (m^3) and Ω is the estuary spring-tide tidal-prism volume (m^3).

To apply this relationship to the Avon-Heathcote Estuary we used the existing Delft3D hydrodynamic model of the estuary (Measures and Bind 2013) to calculate the spring-tide tidal-prism volume under scenarios of pre-and post-earthquake estuary bathymetry and 0.5 m and 1.0 m of sea-level rise⁴. The tidal prism volume was calculated from scenarios modelled in 2017 as part of an assessment of sea-level rise effects on estuary salinity (Orchard and Measures 2017). Note that for this analysis we have used the term ‘spring-tide’ to refer to the largest tides occurring in a typical month rather than a strict definition of astronomic spring tides. Tides on the east coast of New Zealand have only very small spring-neap variations and the largest tides each month are usually ‘perigean tides’ (Walters et al. 2001).

To calibrate the coefficients of the Hicks-Hume tidal-prism vs ebb-delta volume relationship (Equation 2), we estimated the ebb-delta volume using the same approach as Hicks and Hume (1996), differencing the surveyed delta surface from an interpolated “no-delta” surface. For the surveyed surface, we used a digital elevation model (DEM) of the ebb-delta and inlet area that was developed by Measures and Bind (2013) from a compilation of bathymetry data, including their own data at the inlet and data over the ebb-delta and adjacent seabed collected in 1996 by Eliot Sinclair as part of investigations relating to the design and consenting of the Christchurch wastewater ocean outfall pipe⁵.

Any increase in ebb delta size with sea-level rise will require a local sand source. The two available sources are the adjacent beaches and the tidal inlet throat, which is also expected to enlarge with an increased tidal prism. We estimated the throat volume enlargement from the product of throat length (estimated as 600 m off Google Earth Imagery) and increase in throat cross-section area, A_t (m^2), which we estimated off the spring tidal prism using an empirical relation developed from historical data (1854-1964) on the Avon-Heathcote inlet sourced from McPherson and published by Hume and Herdendorf (1988). The relation is:

⁴ We were obliged to use these sea-level rise figures because they are what was input to the Delft3D model.

⁵ Measures and Bind (2013) expended considerable effort in tracking down the survey data for the ocean outfall analysis after Elliot Sinclair struggled to locate it. It was eventually supplied via email by Brett Miller (Water Research Laboratory, School of Civil and Environmental Engineering, University of New South Wales) and only contained data for the estuary and the South Brighton nearshore area.

$$A_t = 6.087 \times 10^{-5} \Omega \quad (3)$$

We estimated the residual sand supply needed from the adjacent beaches as the difference between the increase in ebb-delta volume and the increase in throat volume.

2.3 Potential effects of a major earthquake on the Waimakariri River sand delivery

2.3.1 Landslide scenarios

To investigate the potential effect of a major earthquake on Waimakariri sand delivery we first developed realistic scenarios of potential landslide size, location, and grainsize distributions. To develop scenarios, we systematically inspected (with Google Earth) the catchment of the upper Waimakariri during a workshop with Professor Tim Davies, identifying slopes with the potential for significant landslides. For each potential landslide, the landslide volume was estimated based on slope characteristics. Landslide grainsize distribution was based on surveyed distributions from previously surveyed local landslides (McSaveney and Davies 2007), with the assumption made that future landslides would exhibit similar grainsize distributions.

2.3.2 Time-scale and amount of landslide sand delivery to the coast

Having developed potential landslide scenarios, including the potential volume of sand grade sediment generated, we then considered the timescales with which this landslide derived sand would travel through the river system to the coast. These timescales include (i) the time-varying rate at which landslide deposits are eroded and enter the river system, and (ii) the time taken for the river system to transport sand to the coast.

We estimated the rate of landslide erosion based on published work by Croissant et al. (2017), who used a modelling approach to investigate the erosion of landslides into major river systems. This assumed no time delay before the onset of erosion – such as would occur if the landslides dammed the Waimakariri River, creating lakes and stalling any discharge downstream. To investigate the fill-time of landslide lakes, we estimated landslide dam height and associated impoundment volume, with the lake fill-time equalling the lake volume divided by the median river inflow rate. We assumed that once any such landslide lakes filled and began spilling, the lake outflow would cut quickly down through the landslide material to the original river bed profile, commencing the process of eroding the landslide deposit, and not significantly interrupting the delivery of sediment sourced from upstream.

To investigate the time taken for the river system to transport the landslide sand to the coast, and the rate of sand delivery to the coast, we constructed a one-dimensional morphodynamic model of the lower Waimakariri River. The model extended 70 km from the upper gorge to the coast, as shown in Figure 2-5. Upstream of the model domain the river is confined in a bedrock gorge for approximately 28 km with very little sediment storage, and hence negligible impact on the timing of sediment delivery is anticipated. Several of the potential landslide locations were in, or immediately upstream of, this gorged reach, and the largest landslide (by a substantial margin) was located only a few km upstream from the gorge – hence we consider this a reasonable approximation.

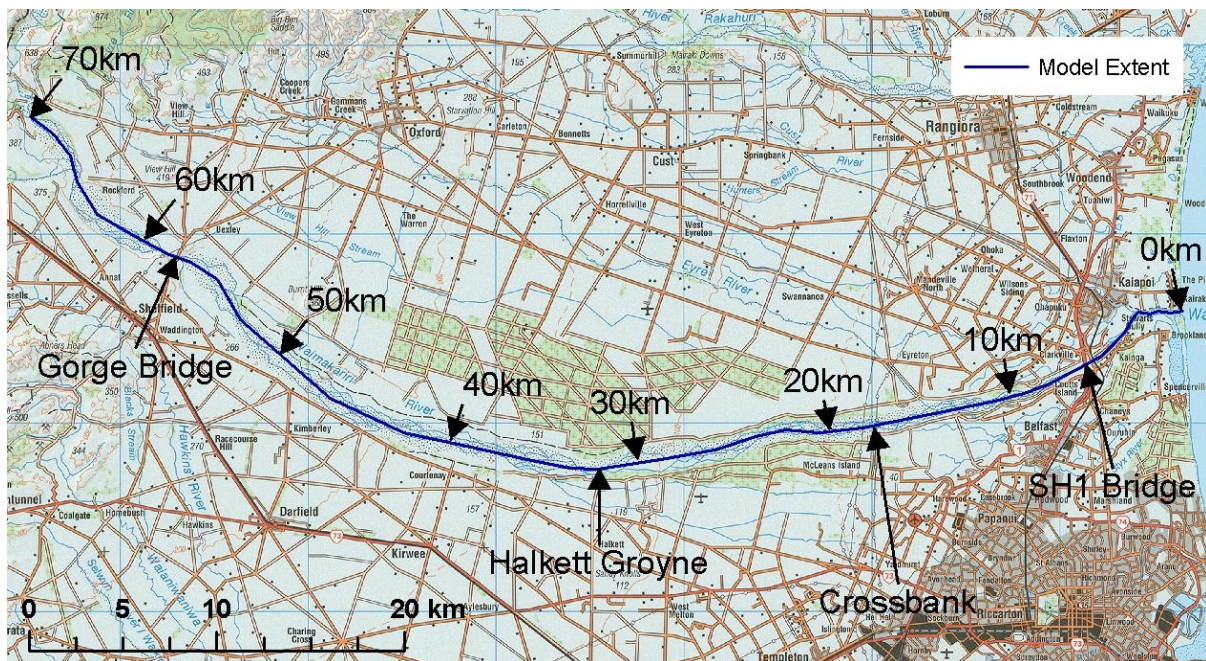


Figure 2-5: Lower Waimakariri River morphodynamic model extent.

The morphodynamic model simulated 40 years of river hydraulics, sediment transport, bed level and bed composition. Model input data was largely taken from a previous calibrated model of gravel transport in the Waimakariri River (Measures 2012). This previous model could not be directly reused for this study because it uses the gravel routing and textural evolution (GRATE) software which does not have the capability to simulate suspended load as well as bedload. This is an important functionality for this study because of the emphasis on fine sand transport. Instead, the modelling carried out for this study used the Sedimentation and River Hydraulics - One Dimension (SRH-1D) software (Greimann and Huang 2018), which was developed by the United States Bureau of Reclamation. Sediment was simulated in six size fractions, ranging from fine sand to cobbles. sediment transport was calculated using the Wu et al. (2000) bed material transport formula which includes suspended and bed load transport. Model inputs are summarised in Table 2-3.

Two scenarios were simulated in the model: a no-landslide (baseline) scenario and a landslide scenario. The landslide scenario assumed: (i) synchronous contributions from all potential landslides, (ii) that all the landslides could be effectively located in the upper gorge (Section 3.3 provides detail that justifies this approximation), and (iii) that transient landslide dams would create no effective delay in sediment delivery. By comparing the two scenarios, the effect of the earthquake derived sediment could be isolated.

Detailed calibration of the morphological model was not within the scope of this investigation. However, a review of published studies into the timescales and magnitude of sediment pulses reaching the coast after previous New Zealand earthquakes was undertaken to sensibility check the modelling conclusions.

The likely river management response to elevated Waimakariri River sediment loads following a landslide in the catchment were discussed with ECan river engineering staff.

2.3.3 Limitations, including potential sediment retention in landslide lakes

The above approach has several limitations, including where landslides would actually occur and their exact size, using an un-calibrated sediment routing model, the extent to which sediment might be retained behind landslide dams should the dams not quickly be incised by the river. These factors all generally contribute uncertainty to the supply of landslide-derived sand and the amount of sand retained in storage, and have less impact on the time-scale of landslide sand delivery to the coast, which is the primary focus of our investigation.

The sediment retention factor could be significant. Although counterintuitive, a landslide can potentially cause a reduction in river sediment supply if it forms a long-lasting dam and lake that traps sediment from upstream. A New Zealand example of this is the landslide dam in the Mokihinui River gorge which fell during the Buller earthquake (Adams 1981). This landslide initially impounded a lake (Lake Perrine) which was 20 m deep and 11 km long. Part of the dam washed out naturally but the lower 12 m remained and caused sediment from upstream to be trapped, eventually filling the lake. The likely reason the Mokihinui landslide dam was able to persist when most other landslide dams on major rivers are rapidly eroded is that it had a large proportion of boulders (by virtue of the local geology).

To investigate the likelihood of landslide dams impounding sediment in the Waimakariri, we analysed the potential maximum size of lakes which could be formed by the potential landslides identified and considered their likely longevity and capacity to trap sediment.

Table 2-3: Input data for the morphodynamic model of the lower Waimakariri River.

Model Input	Source data
Cross-sections	Cross-sections copied from pre-existing GRATE model (Measures 2012). Majority of cross-sections were originally derived from Environment Canterbury surveys.
Roughness	Manning's roughness coefficients taken from calibrated previous model (Measures 2012).
Inflow	Simplified annual flow hydrograph developed from observed long term average flow duration curve at Old Highway Bridge flow recorder. This synthetic hydrograph was used to avoid confusing the landslide effects on sediment load with those due to inter-annual hydrological variability.
Downstream hydraulic boundary	Tidally varying water level derived from astronomic tide constituents.
Baseline (i.e., no-landslide) fine sand sediment input	Fine sand input was calculated from river flow using the sediment rating derived for stage A of this study (Hicks et al. 2018).
Baseline (i.e., no-landslide) coarse sand and gravel sediment input	Coarse sediment input was set at 300,000 m ³ /yr based on previous analysis of gravel transport (Boyle and Surman 2009). This is consistent with previous modelling of gravel transport in the Waimakariri (Measures 2012). Flow related variability in sediment input was based on a scaling of the fine sediment rating, so as to achieve 300,000 m ³ /yr total input. The size distribution of coarse sediment feed was taken from the pre-existing GRATE model (Measures 2012) and originally derived from bulk sediment samples.
Landslide sediment feed rate and size grading.	From analysis conducted for this study, as described in Section 3.3.
Initial condition surface and sub-surface bed composition	Initial condition surface and sub-surface grain size distributions were set based on the pre-existing GRATE model (Measures 2012).

2.4 Impacts of future sand budget changes on future beach volumes and shoreline position

The effects of the possible future changes to the sediment budget components (and of their various combinations) on beach volumes and consequently on shoreline position were assessed using a spreadsheet-based sediment budgeting model built for the study shore.

2.4.1 Model development

As schematised on Figure 1-1, the City shore between the Waimakariri River mouth and Sumner is prograding (advancing seaward). This occurs because the external sand supply provided by the Waimakariri River is more than enough to overcome the sand demand to counter the effect of a rising sea-level.

Setting aside sea-level rise effects and considering only the case of a prograding span of shore of length B (representing the shore length between the river mouth and Sumner in metres), as on Figure 2-6a, the total sand volume supply rate from the river (V_r , m^3/yr) required to prograde the profile seaward at rate Δy_r (m/yr) is $V_r = \Delta y_r H B$, where H (m) is the profile height above the closure point, which is the sum of the dune height (D_b , m) above mean sea-level (MSL) and the closure depth below MSL (D_o , assumed here as the Hallermeier outer limit, m). Rearranging, $\Delta y_r = V_r / (H B)$.

With sea-level rising at rate S (m/yr) and no external sand supply, as in Figure 2-6b (i.e., $V_r = 0$), the “Bruun rule” (Bruun 1962) assumes the sand volume demand rate (V_s , m^3/yr) required to lift the profile vertically to match the sea-level rise to retain an “equilibrium” profile over profile width L (m) is $V_s = S L B$, where L is the sum of the beach width above MSL (L_b) and the width of the submerged profile out to the closure depth (L_o). It also assumes that the shore must retreat until the sand volume yielded by the retreat (equal to $-\Delta y_s H B$) matches the sand demand to lift the profile, hence $V_s = S L B = -\Delta y_s H B$. Rearranging gives the “Bruun Rule”:

$$\Delta y_s = -SL/H \quad (4)$$

With both a river sand supply and a rising sea-level, the net rate of shoreline shift (Δy) becomes:

$$\Delta y = \Delta y_r + \Delta y_s = (V_r / BH - SL/H) \quad (5)$$

If the river supply V_r matches the sea-level-rise demand V_s , then profile lift occurs without any retreat. If $V_r > V_s$, then the profile will continue to prograde but not as quickly as it would without a rising sea-level.

Following Hicks et al. (2018) and as shown in Figure 2-7, for the City shore V_r can be set equal to the supply of Waimakariri River sand delivered to the beach profile south of the Waimakariri River mouth. Therefore, $V_r = Q_s T_e P_s$, where Q_s is the total river sand supply to the coast (m^3/yr), T_e is the proportion (or trap efficiency) of this river sand retained on the beach profile, and P_s is the proportion of the retained sand that is transported south from the river mouth to the City shore. Thus:

$$\Delta y = (Q_s T_e P_s / BH - SL/H) \quad (6)$$

It follows that a stable shoreline (i.e., $\Delta y = 0$) occurs when $Q_s T_e P_s / B = SL$, or when

$$S = Q_s T_e P_s / BL \quad (7)$$

Equation (7) indicates, for example, that under the current river supply and wave climate (using $Q_s = 745,000 \text{ m}^3/\text{yr}$, $T_e = 0.36$, $P_s = 0.68$, $B = 20,650 \text{ m}$, and $L = 750 \text{ m}$ from Hicks et al. 2018), the City shore would only begin to retreat overall when the rate of sea-level rise exceeded 12 mm/yr .

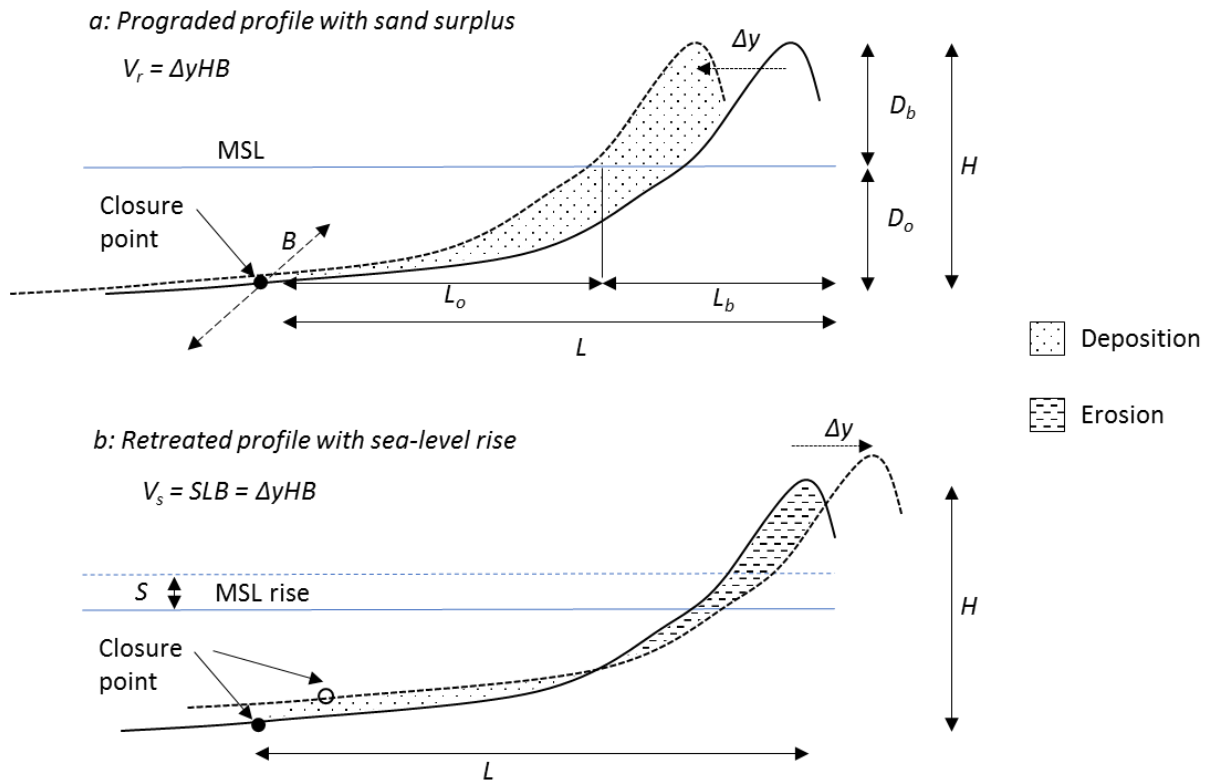


Figure 2-6: Schematic of shore budgeting model. a: Case of a prograding shore receiving a sand surplus. b: Case of an equilibrium shore responding to rising sea-level. Symbols as defined in text. Note B is the beach length alongshore.

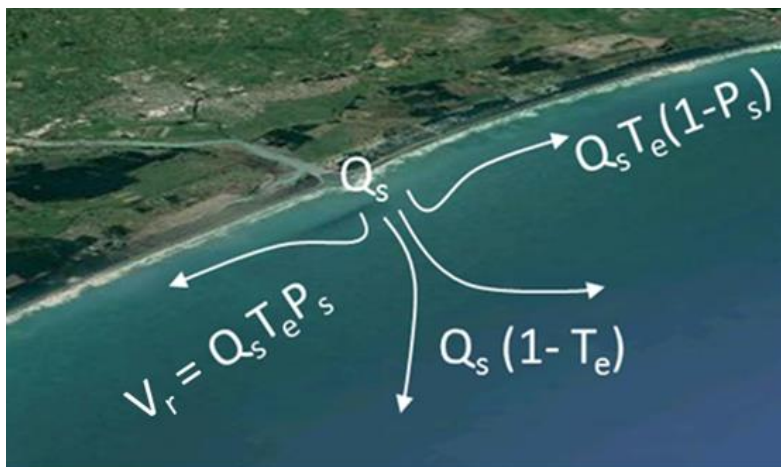


Figure 2-7: Budget of sand distribution from the Waimakariri River mouth. Q_s is river sand load, T_e is the proportion of river sand retained on the beach profile, P_s is the proportion of sand transported southwards from the river mouth, and V_r is the net volume supply rate of river sand to the shore south of the river.

2.4.2 Model application

For this study, Equation (6) was used to estimate the spatially-averaged shoreline advance/retreat rate along the 20.65 km of shore between the Waimakariri River mouth and Sumner, using the spatially averaged profile height (H) and width (L), under a suite of scenarios associated with different future river sand supplies, nearshore wave climate, and sea-level rise (which impact on the terms Q_s , P_s , D_o , L_o , and S in the above equations). The spatial averaging of H and L was done using their values estimated at each of the 41 ECan profile locations between Brooklands Spit and Sumner Head, weighted by the span of shore each profile represents.

For L , the beach width (L_b) component was taken as 100 m all along the shore (as done in the Stage A report). The submerged width (L_o) was calculated based on (i) the estimated closure depth derived from analysis of the SWAN wave modelling for the various nearshore wave scenarios (Section 2.2.5) and (ii) a submerged profile shape modelled with a Dean-type equation (Dean 1991):

$$Z = A Y^{2/3} \quad (8)$$

where Z is the water depth (m) below mean sea level (MSL), Y is distance offshore from the MSL shoreline, and A is an empirically-fitted parameter that reflects the wave climate and beach sediment grade.

For this study, values of A were fitted to the profiles at Beatty Street and Spencer Park (see Figure 1-1 for locations) plotted by Allan et al. (1999), reproduced here in Figure 2-8. A -values of 0.0878 and 0.116 were derived for these two locations, respectively, using a linear-regression fit to plots of Z vs $Y^{2/3}$ (Figure 2-9). The higher A value at Spencer Park, indicating a slightly steeper profile, is consistent with the slight trend for northward increasing beach grainsize observed between Southshore and the Waimakariri River in the ECan dataset (Hicks et al. 2018). We varied A linearly between Beatty Street and Spencer Park but assumed that $A = 0.0878$ between Sumner and Beatty Street and $A = 0.116$ between Spencer Park and the Waimakariri Mouth.

The dune height, D_b , values were temporal averages taken from the ECan beach profiles. The profile height, H , is the sum of D_b and the wave-climate-dependent closure depth, D_o .

Following Hicks et al. (2018), the proportion of river sand transported south from the Waimakariri River mouth (P_s) under the various nearshore wave scenarios was taken as the ratio of southward longshore transport potential to gross longshore transport potential at the river mouth, averaged over five SWAN model output stations along a 2.65 km span of shore centred at the river mouth. The nearshore sand trapping efficiency, T_e , was assumed constant at 36% for each scenario assessed (as derived by Hicks et al. (2018) based on matching the size grading of the river sand load with the size grading of the beach sand).

2.5 Effects of future sand budget changes on river and estuary mouth stability and coastal flooding

We undertook a brief qualitative assessment of river mouth and inlet stability and coastal flood risk based on the assessments of changes to the individual sediment budget components and the consequent impact on shore stability.

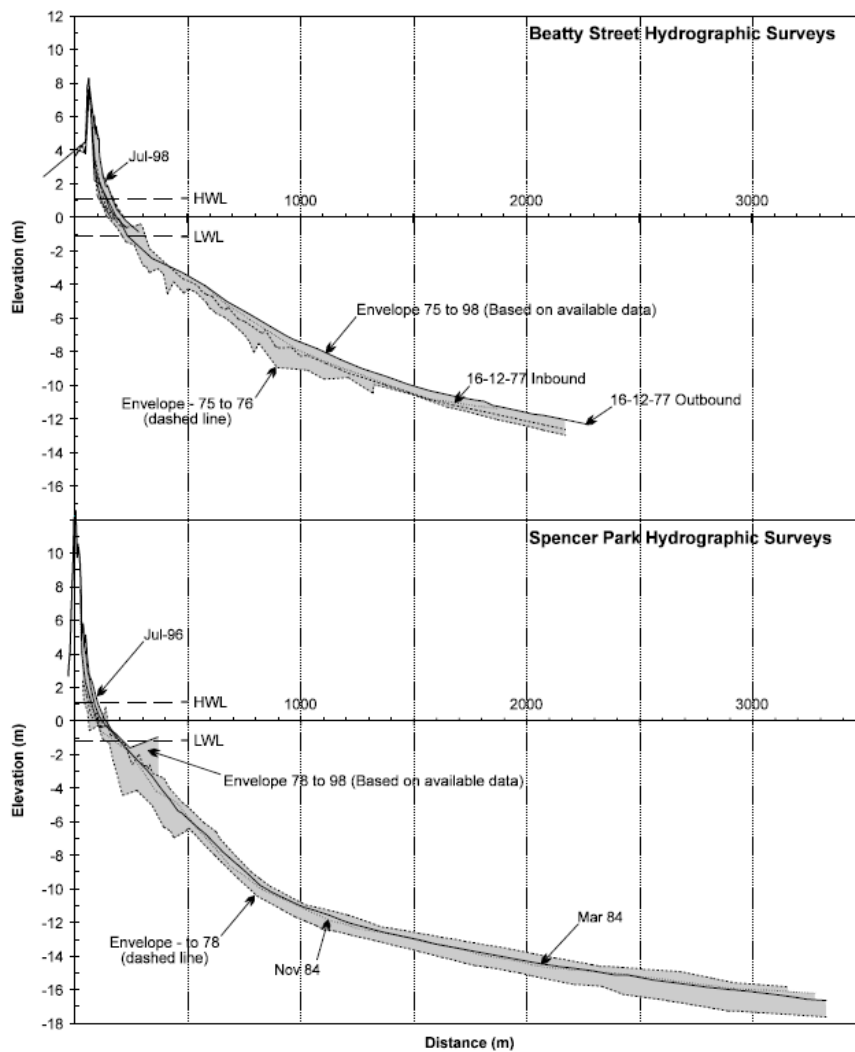


Figure 2-8: Offshore profile surveys at Beatty Street and Spencer Park. From Allan et al. (1999).

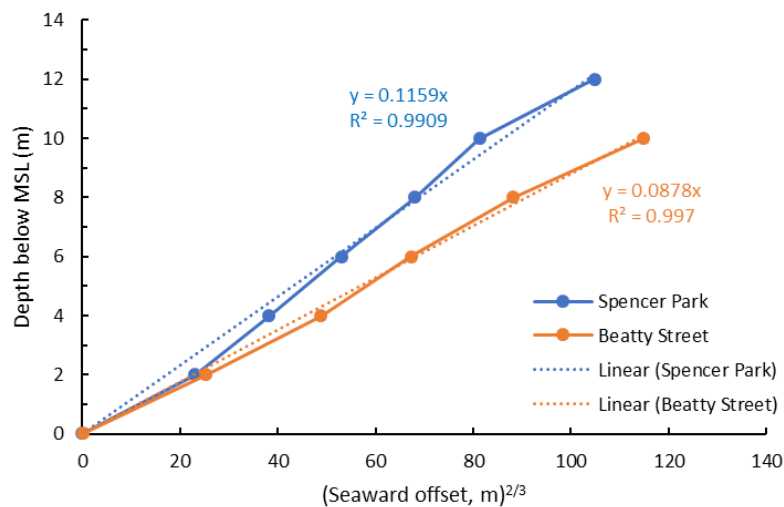


Figure 2-9: Beatty Street and Spencer park profiles distance-offshore scale transformed to the power of $2/3$. The regression slopes provide values for the A-parameter in the $Z = AY^{2/3}$ "Dean profile". The profiles were digitised from the mid-range of the profile envelopes shown in Figure 2-8.

3 Results

3.1 Climate change effects on Waimakariri River supply of beach sand

3.1.1 Projected annual suspended loads from TopNet modelling coupled with climate change scenarios

The results of the projected future suspended loads from the TopNet modelling with climate change are given in Figure 3-1 and Table 3-1. Figure 3-1a shows the time-accumulated suspended load under the RCP2.6 scenario from all six GCMs. By 2100, the accumulated loads diverge by $\pm 17.5\%$ about the accumulated load averaged from the six GCMs (140 Mt). This gives a measure of the uncertainty associated with using different GCMs. Similar divergences of predictions (not shown) are associated with the other RCP scenarios. There is little difference between the curves of the median and mean of the six GCM results, so we focussed further comparisons on the GCM result means.

Figure 3-1b shows the mean time-accumulated suspended load under the four RCP scenarios. There appears to be little difference among them except that the annual loads of the RCP8.5 scenario trend lower than the others (by about 8%) until 2075, but thereafter the RCP8.5 loads increase.

Figure 3-1c, showing the 10-year running-average suspended loads, again shows little difference among the scenarios and only suggests a time trend for increasing load with the RCP8.5 scenario.

Table 3-1 confirms that the only scenario with a statistically significant time-trend in the 10-year running-average load is RCP8.5, with a time trend that results in a 28% increase in load between 2006 and 2100. Interestingly, even though the time-trends on the other scenarios are not statistically significant, their relative values make some sense in terms of the associated human effort in changing greenhouse gas emissions (as in Table 2-1). Thus: RCP2.6, involving the most aggressive attempt at reducing emissions, projects a 7% reduced load by 2100; RCP4.5 a similar reduction; RCP6.0 a marginal increase under a higher stabilised emission rate; and RCP8.5 the largest increase with unmitigated emissions.

Table 3-1 also shows insignificant difference in the long-term (2006-2100) average suspended loads among the scenarios, with the standard error on each scenario's average (0.04 Mt/yr) being the same as the range between them.

It is of note that all the projections show annual suspended loads (about 1.5 Mt/yr) approximately half the measured average annual suspended loads (about 3.0 Mt/yr) reported by Hicks et al. (2018) – which raises significant questions around the reality of the flows that have been simulated via the GCM-RCM-TopNet modelling chain.

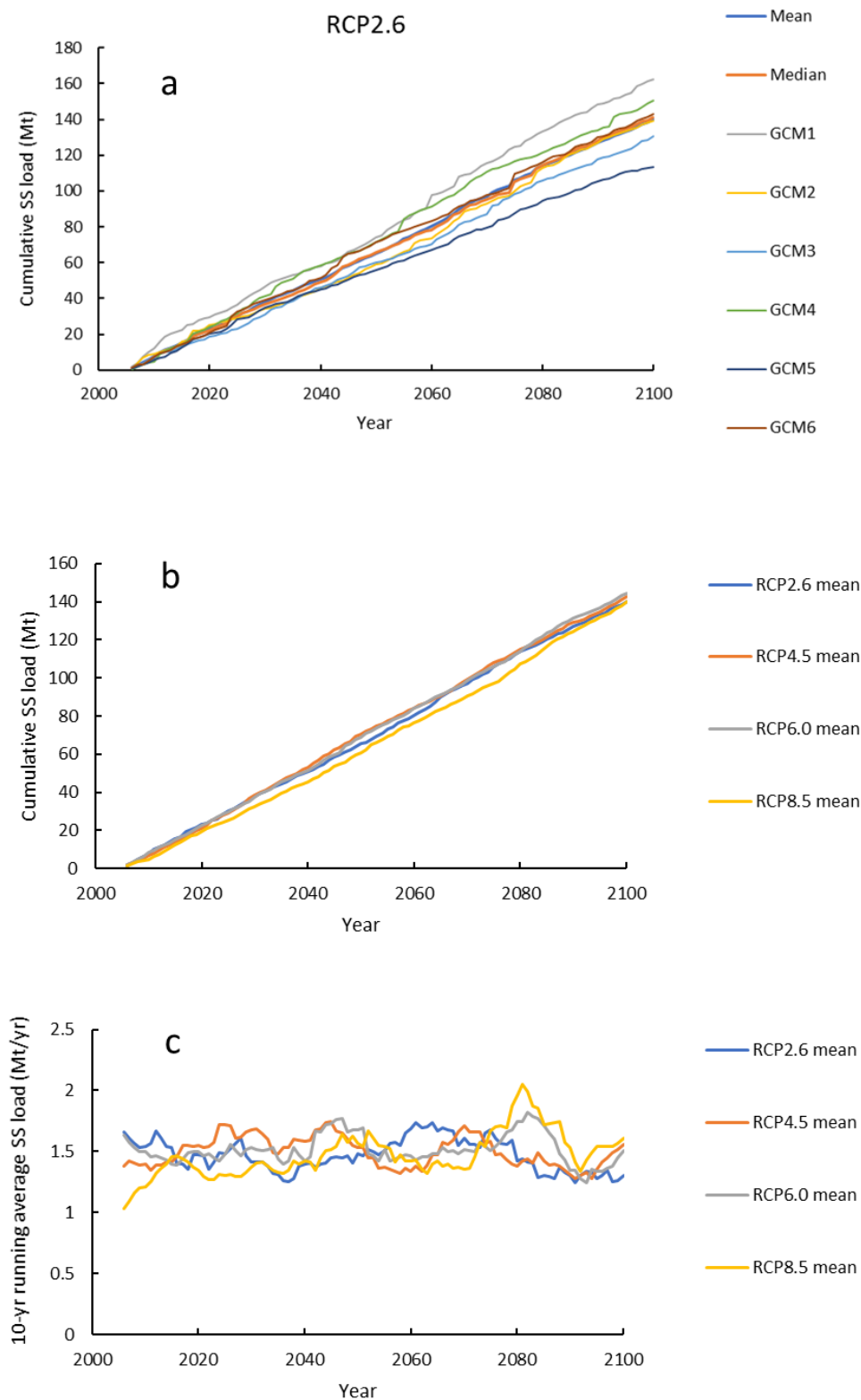


Figure 3-1: Projected future Waimakariri suspended loads from TopNet modelling with climate change scenarios. a: Cumulative loads for RCP2.6 scenario for the six different GCMs. b: Cumulative loads averaged over the six GCMs for RCP2.6, RCP4.5, RCP6.0, and RCP8.5 climate change scenarios. c: 10-year running average loads averaged over the six GCMs for each scenario.

Table 3-1: GCM-averaged long-term average suspended load by climate change scenario, and time-trend statistics. The time trend is expressed as the annual change in the 10-year running average load relative to the long-term (2006-2100) average load. Statistically significant trends at the 5% level are identified in bold. The fifth column indicates the change by 2100 from the current long-term average load.

Scenario	Long-term average suspended load (Mt/yr)	Standard error on long-term average (Mt/yr)	Time-trend on 10-year running average (as % per year of long-term average)	% change in 10-year running average load 2006-2100	r^2 on time trend
RCP2.6	1.47	0.04	-0.07%	-7.0%	0.056
RCP4.5	1.50	0.04	-0.09%	-8.1%	0.082
RCP6.0	1.52	0.04	0.00%	0.1%	0.0002
RCP8.5	1.47	0.04	0.30%	28.1%	0.43

Reliability-check on TopNet modelled flow records under climate change scenarios

A validation check on the simulated flows from the climate change realisations was undertaken for the period 1/6/2008 through 1/6/2016, when observed flow data was available from the Otarama gauge. Figure 3-2 compares the observed hydrograph for this period with hydrographs simulated from three GCM realisations of the RCP2.6 Scenario. What is immediately clear is that event peak flows are much smaller than those observed, while the simulated hydrographs also show a stronger seasonal signal (with highest baseflows in spring) than does the observed hydrograph. The other scenario-GCM combinations show similar patterns. Table 3-2, shows that while the mean flows were not too dissimilar to the observed flows (typically 5-7% higher), the modelled flow maxima were around one third the observed maximum flow.

This high-flow validation issue features in a comparison of flow-duration curves (Figure 3-3), which shows, for the example cases of the RCP2.6 and RCP8.5 scenarios, that the curves from the simulated records diverge markedly from the observed curve at flows above about 500 m³/s. The other scenario-GCM combinations have similar curves. Because a sizable proportion of the suspended sediment transport in the Waimakariri occurs during higher flows (see Figure 3-2 of Hicks et al. 2018), the reduced frequency of high flows in the simulated records explains why their associated suspended sediment loads are only about half the loads calculated when the same rating curve is combined with the observed flow record.

It is likely that all components of the GCM-RCM-TopNet modelling chain contribute to this high flow validation issue, but a significant contributor appears to be the TopNet model calibration, which apparently focussed on replicating mean flows rather than extremes (C. Zammit, NIWA, pers. comm.). Unfortunately, it affords little confidence in the absolute sediment load results generated. At best we can conclude from the relative differences between the RCP scenarios that (i) changes in the Waimakariri suspended sediment load (and by inference the Waimakariri sand load) by 2100 due to climate change could range from a 7-8% decrease (RCP2.6 and RCP4.5) to a 28% increase (RCP8.5), and (ii) that these figures are very uncertain.

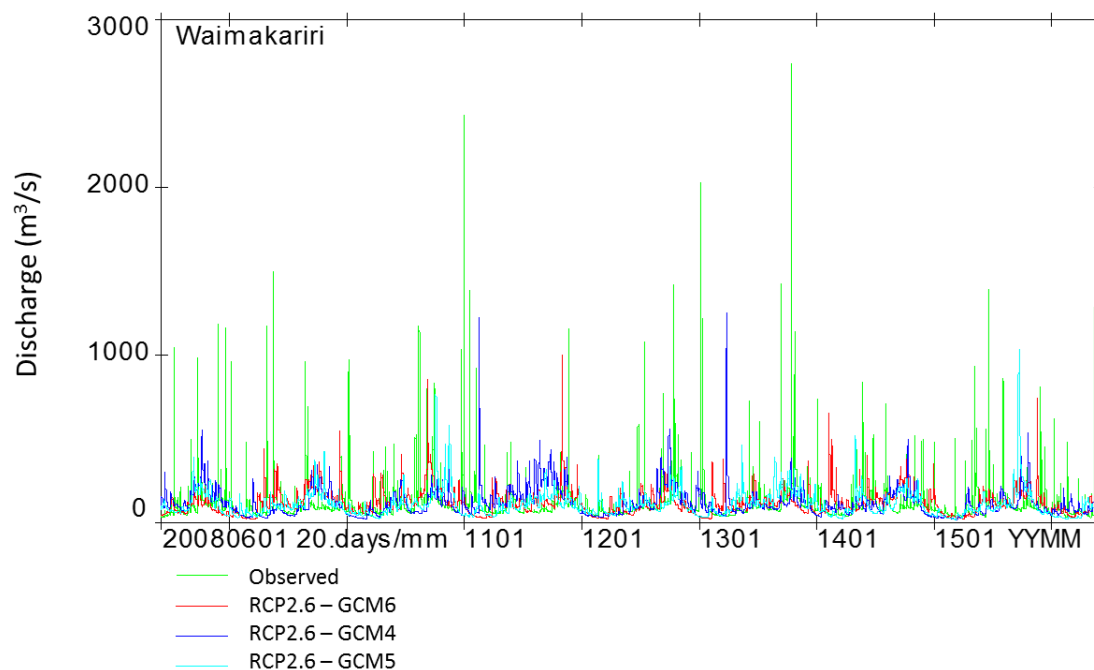


Figure 3-2: TopNet-modelled hydrographs of Waimakariri at Otarama flows for 2008-2016 for three GCM realisations of the RCP2.6 climate change scenario, compared with observed flows. Note much smaller flood peaks and stronger seasonal variation with modelled flows.

Table 3-2: Means and maxima of TopNet-modelled Waimakariri at Otarama flows for 2008-2016 for the six GCM realisations of the RCP2.6 and RCP4.5 climate change scenario, compared with mean and maximum.

Scenario-GCM	Mean (m³/s)	Maximum (m³/s)
Observed	114	2745
RCP2.6-1	140	1170
RCP2.6-2	124	625
RCP2.6-3	114	930
RCP2.6-4	121	1257
RCP2.6-5	113	1037
RCP2.6-6	122	1006
<i>Average</i>	<i>122</i>	<i>1004</i>
RCP4.5-1	120	679
RCP4.5-2	110	1306
RCP4.5-3	122	1300
RCP4.5-4	132	677
RCP4.5-5	117	587
RCP4.5-6	116	739
<i>Average</i>	<i>120</i>	<i>881</i>

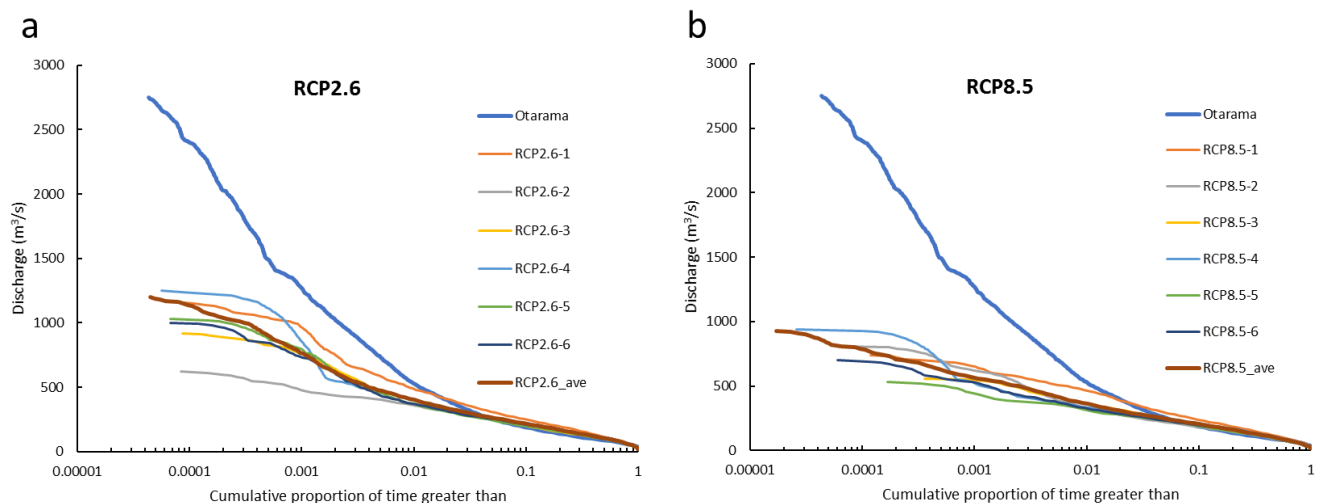


Figure 3-3: Flow-distribution curves at Waimakariri at Otarama for period 2008-2016 for TopNet-modelled outputs of GCMs for (a) RCP2.6 and (b) RCP8.5 climate change scenarios, compared with observed flow duration curve.

3.1.2 Changes in Kidson Weather Types

According to Smart et al. (2018), under the current climate five Kidson Weather Types occur most frequently and produce the heaviest rain in Canterbury: TNW, T, SW, and TSW (all representing weather systems associated with low pressure troughs) and NE (which occurs when a blocking anticyclone directs a NE airstream onto Canterbury). Of these, it is the TNW type, associated with “nor’ wester” conditions, that generates the heaviest rainfall in the Waimakariri catchment. This is concentrated in the headwaters, close to the main divide, and has the greatest impact on sediment delivery to the coast. Figure 3-4 shows that while the upper Waimakariri catchment (i.e., upstream from the Waimakariri Gorge) contains only 51.6% of the total catchment area, it generates 81.8% of the runoff and 86.8% of the suspended sediment load. The other weather types tend to produce more rain on the coastal plains and front ranges but do not contribute substantively to the Waimakariri runoff and sediment load.

Smart et al. (2018) used the results of the RCM runs of Mullan et al. (2016), based on output from the same six GCMs as used in Section 3.1.1, to project changes in the frequency of the Kidson Weather Types under the RCP4.5 (“middle-of-the road”) and RCP8.5 (“large CO₂ increase”) climate change scenarios at the “end-of-century” (2071-2100). They concluded that the TNW type would tend to decrease in frequency during the spring (more so under the RCP8.5 scenario) - which implies, if anything, some reduction in the amount of Waimakariri runoff and sediment load during spring freshes and floods. No conclusion could be drawn for the other seasons because there was no change in TNW type frequency that was consistent across all six GCMs.

It should be noted, however, that while there may be a future reduction in the frequency of NW events, it is generally accepted that rainfall extremes will increase in intensity due to atmospheric warming associated with climate change and to changes in storm dynamics (Smart et al. 2018). This increase in intensity may well counteract, or even prevail over, the effect of any decrease in event frequency on catchment erosion rates.

Thus, in regard to future Waimakariri Catchment erosion rates we can draw no useful conclusion from the assessment of future change in weather type frequency: the erosion rates could be lower, higher, or unchanged.

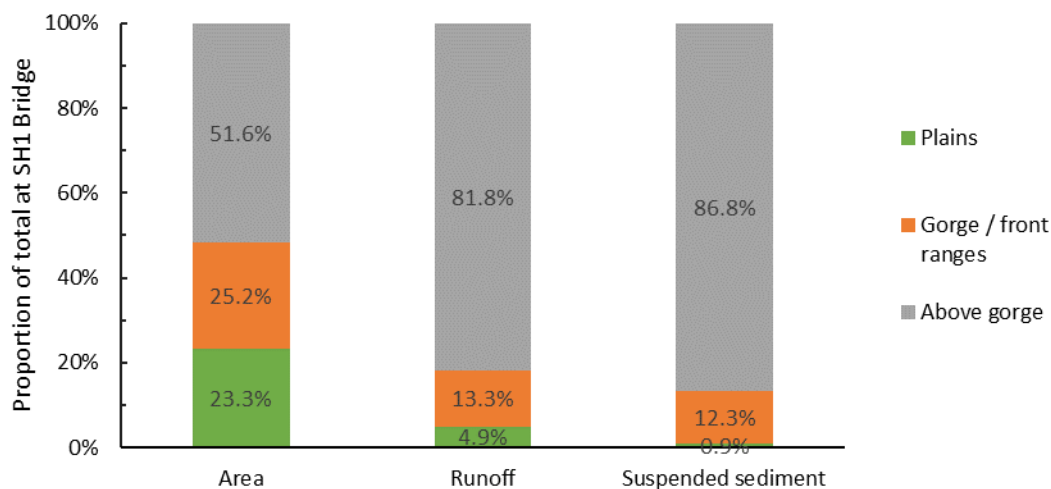


Figure 3-4: Proportions of catchment area, runoff, and suspended sediment load associated with the upper (above gorge), middle (gorge and front-ranges), and lower (Canterbury Plains) parts of the Waimakariri Catchment. Runoff proportions based on Woods et al. (2006); suspended load proportions from model developed by Hicks et al. (2011).

3.1.3 Regional projections of hydrological change from national guidance documents

MfE (2016a) produced maps of New Zealand showing projected changes in seasonal precipitation under the four climate change scenarios listed in Table 2-1. These showed increased winter (June, July, August) and spring (September, October, November) precipitation over the upper Waimakariri catchment, with the larger increases occurring in winter, but less precipitation in the other seasons. The changes were systematically larger going from the RCP2.6 (10-15% increase in winter) through RCP8.5 (20-30% increase in winter) scenarios. However, the net changes over all seasons were relatively small, as shown by the maps in MfE (2016b) – reproduced here in Figure 3-5 – which suggest changes in annual precipitation of no more than +10% in the upper Waimakariri and little change in the middle catchment under the RCP8.5 scenario, and less change under the RCP2.6 scenario.

Hicks et al. (2011) found that sediment yields (Y , t/km²/yr) around New Zealand relate non-linearly to mean annual precipitation (P , m/yr) as $Y = A P^{1.7}$ (where A is a coefficient that depends on the susceptibility of the terrane to erosion). Assuming this relationship holds across the Waimakariri, then a 10% increase in annual precipitation should result in a 17% increase in sediment yield.

MfE (2016a and b) note that rainfall intensities should generally increase with climate change, particularly where the mean annual rainfall increases, such as in the South Island. They note that intensities may increase even where the annual totals decrease. With no change in annual rainfall, increased rainfall intensity should increase erosion and intensify runoff, hence should result in an increased sediment yield. However, the degree of increase in sediment yield is challenging to predict.

It remains to conclude from the MfE reports that through the combined effects of increased annual rainfall and increased rain intensity in the upper Waimakariri Catchment, the Waimakariri River's

sediment load could increase by something more than 17% under the RCP8.5 scenario by about the end of the century, with less change anticipated for the other scenarios. This bluntly aligns with the result derived from the Waimakariri TopNet simulations reported in Section 3.1.1 (which is not surprising given that the assessments here and in Section 3.1.1 are based on the same downscaled GCMs of the same RCP scenarios).

Collins and Zammit (2016) used the same set of climate change modelling results to project changes in mean annual flood size using an uncalibrated TopNet model of all New Zealand⁶. This showed (Figure 3-6) larger mean annual floods across most of the Waimakariri Catchment, particularly under the high emissions RCP8.5 scenario – which also portends increased sediment yields but only qualitatively.

Annual average change in rainfall (%) by 2090 under RCP2.6 (left) and RCP8.5 (right)

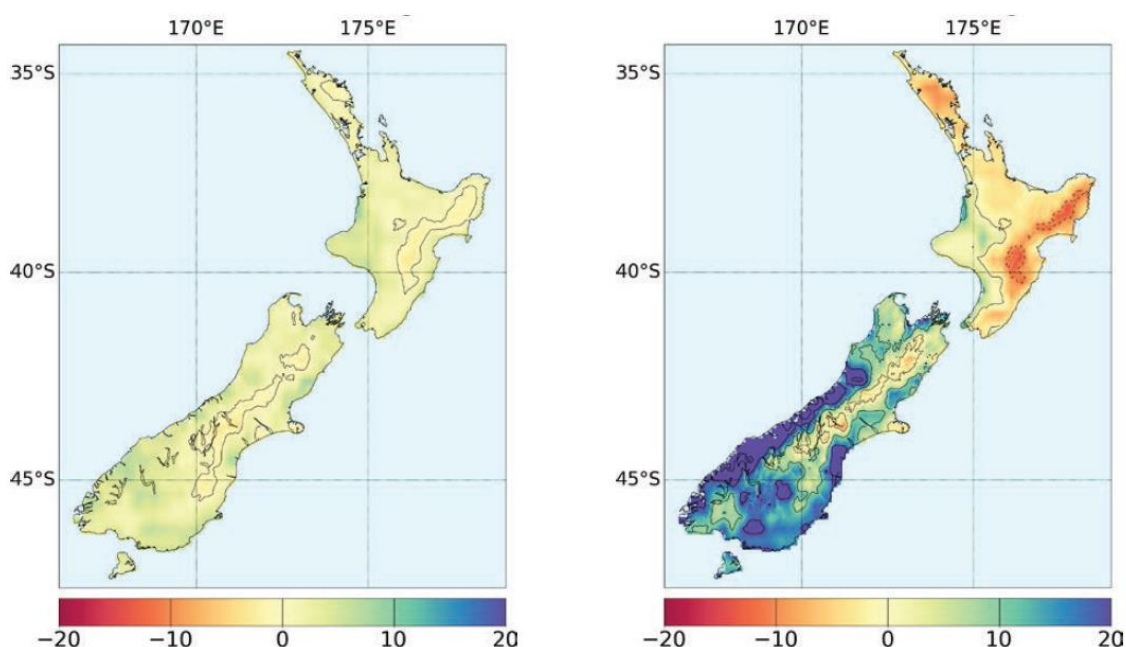


Figure 3-5: Projected % changes in average annual rainfall by 2090 under the RCP2.6 (low emissions) and RCP8.5 (high emissions) climate change scenarios, relative to 1995 baseline. Reproduced from MfE (2016b).

⁶ A different model from the calibrated TopNet model of the Waimakariri Catchment reported in Section 3.1.1.

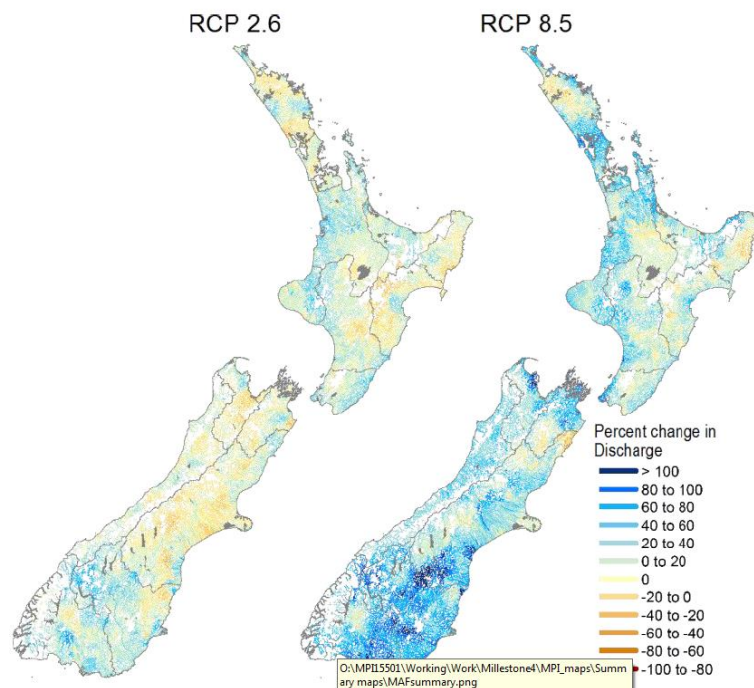


Figure 3-6: Late-century % changes (median across multiple GCMs) in mean annual flood for RCP2.6 (low emissions) and RCP8.5 (high emissions) climate change scenarios. From Collins and Zammit (2016).

3.1.4 Changes in land cover

Climate-change-driven changes in land cover also have the potential to alter erosion rates and sediment generation. However, in the Waimakariri case where the bulk of the sediment-generating area of the catchment has a cover of bare rock/scree, native tussock, or native forest and the land use is non-agricultural, land cover is not expected to change significantly – either as a natural response to altered climate factors or as a human response with land use.

3.1.5 Changes in gravel extraction rates

As explained in the Stage A report (Hicks et al. 2018), substantial gravel extraction has occurred in the Lower Waimakariri River, upstream of SH1 Bridge, for at least the past 60 years. This extraction is required by ECan to manage the natural aggradation trend and maintain a riverbed profile that preserves the flood-carrying capacity of the channel. Eleven percent of the riverbed material in the gravel extraction reach is sand, thus the extraction removes sand from the river channel (at a rate averaging 38,000 m³/yr, which is equates to about 5% of the sand discharge to the coast). However, even if the extraction was stopped, the equivalent amount of sand would be deposited in the aggrading river bed and would not reach the coast. While this sand loss by extraction (or by deposition in the absence of extraction) is technically a deficit in the river's sand budget in the extraction reach, this deficit will have been captured in the sediment gaugings undertaken within the past 60 years at the old SH1 highway bridge (which is at the downstream boundary of the extraction reach). Thus, in the Stage A report, sand losses to extraction were not subtracted from the measured sand discharge past the old SH1 bridge (746,000 m³/yr)⁷.

⁷ Although, as shown on Figure 1-1, the current sand losses to extraction and to irrigation takes further upstream may be added to the 746,000 m³/yr sand at SH1 Bridge to estimate a sand load from the mountains totalling 792,000 m³/yr.

In the future, rates of gravel extraction from the Lower Waimakariri channel are expected to match future rates of gravel delivery from upstream, since it will still be necessary for ECan to maintain long-term average design bed levels and associated flood conveyance and protection. Thus, any increase in gravel bedload delivery from up-river associated with climate change and more intense river flows will be matched by increased gravel extraction. Moreover, at least to a first approximation, the proportional increase in bedload and extraction (say $x\%$) can be expected to be matched by the same proportional increase in suspended load. Thus, the effects of future changes in extraction will remain accounted for in the load at the old SH1 bridge, which should also increase by $x\%$. In other words, extraction effects will be implicitly included in any proportional increase in catchment sediment load applied to the reference sand load figure at the old SH1 bridge.

3.1.6 Changes in sand diversion with irrigation water abstraction

Water management decisions in Canterbury, including those relating to water abstraction from rivers, are conducted within the framework of the Canterbury Water Management Strategy (Canterbury Mayoral Forum 2009). The Waimakariri River lies in the Waimakariri Water Zone, and its strategic management decisions are made collaboratively by the Waimakariri Zone Committee. One of the Zone Committee's agreed aims is to investigate options to improve irrigation reliability to 95% and increase the irrigated area by up to 50,000 ha (Waimakariri Zone Committee 2012). Climate-change expectations on the Canterbury Plains are for drier summers (Collins and Zammit 2016), so if anything, climate change is liable to increase this irrigation water demand.

Low flows in the Waimakariri are currently fully consented, meaning that any further abstraction would need to involve "flood harvesting" from less reliable high flows. Various water storage schemes of different designs and sizes have been proposed. However, all schemes have a similar basis in that they allow the harvesting of more water during periods of high flow to be stored for use during periods of low flow when further abstraction is not appropriate.

To assess the effects of potential additional water abstraction on the sand load in the Waimakariri River, we have assumed that sufficient off-channel water storage will be developed to facilitate irrigation of an additional 50,000 ha. The Waimakariri River is not the only source of water to the Waimakariri Zone but it is the largest and it has the most potential for additional extraction, so we have assumed that all this water is supplied from the Waimakariri River. These assumptions are conservative and represent a maximum scenario for water abstraction.

Waimakariri Irrigation Limited currently supply water to their farmer shareholders at a rate of 0.525 l/s/ha (equivalent to approximately 4.5 mm/day). Assuming a similar supply rate for the additional irrigated area, this equates to an average water supply rate during the irrigation season of 26 m³/s, equating to a total volume of approximately 400 million m³ per irrigation season (assuming six months of irrigation).

The average 26 m³/s rate of additional river water abstraction required is similar to the sum of the current takes (~24 m³/s), but the additional abstraction would be focussed at higher flows (we assume between the mean flow and 1,000 m³/s). We note that this future take scenario is similar to the consented but unused Central Plains water take (current take is 2 m³/s, consented take is 25 m³/s, no immediate plans to utilise this additional consented amount). This demonstrates that while our additional abstraction scenario is somewhat conservative it is still realistic.

Based on the above scenario for additional water abstraction, and following the approach outlined in Section 2.1.2, the additional suspended sand load diverted from the Waimakariri River was

calculated to be 36,000 t/yr, equivalent to 3% of the current sand load in the river and approximately 2.5 times as much as is currently removed.

The actual amount of sand removed from the river will depend on the design of the water intakes and their operation. All major water intakes have sediment traps to prevent sand entering canals and storage reservoirs. Most modern sediment traps return the sand to the river periodically, either by flushing or by mechanical excavation (e.g., Central Plains Water Waimakariri intake at Sheffield). However, other sediment traps (e.g., the Waimakariri Irrigation intake at Browns Rock and the Paparua Scheme intake) do not return trapped sand to the river but dispose of it elsewhere. If all future water abstraction operations returned intercepted sand to the river, then there would be no impact to the river sand load.

Thus, we project that increased future irrigation takes could reduce the Waimakariri sand load by between zero and 3%. Since this future additional sand removal by irrigation takes is independent of future changes in sand supply from up-catchment, we consider it should be extracted explicitly from the sand load estimated at the old SH1 bridge.

3.1.7 Sand entrapment in the tidal reach of the Waimakariri River

As explained in Section 2.1.3, we expect that sand deposition will occur in the tidal reach of the Waimakariri River to lift the bed to match the rise in sea-level. The present tidal reach covers an area of approximately 664,000 m² (as measured off aerial imagery), thus a 2 mm/yr rate of sea-level rise (status quo rate) would deposit 1,300 m³/yr, a 5.4 mm/yr sea-level rise (corresponding to a 0.55 m rise by 2120 if this were the average rise) would deposit 3,600 m³/yr, and a 13 mm/yr average rise (corresponding to a 1.36 m rise by 2120) would deposit 8,800 m³/yr. We discounted the river sand discharge to the coast by these volumes in the sand budget analysis.

3.1.8 Review of Tonkin & Taylor (2017) assessment

Tonkin & Taylor (2017) assumed a 10% reduction in the Waimakariri River's sediment supply by 2065 and a 30% reduction by 2120 due to climate change effects. These figures were underpinned by the assumption that the Waimakariri's response would be like that of the Rhine River, which was comprehensively investigated for climate change impacts by Asselman et al. (2000).

Tonkin & Taylor considered the Rhine would be a suitable 'model' for the Waimakariri because both *"are snow-fed transitioning from an alpine environment to a flood plain and have similar mean flood flows (2000-2500 m³/s for the Waimakariri River and 2,300 m³/s for the Rhine River)"*. They noted (from information in Asselman et al. 2000) that most of the Rhine's sediment load is transported during mean flow conditions rather than during flood flows, and that the Asselman et al. analysis indicated that the sediment supply to the lower Rhine could reduce by 5-40% as a result of climate change and land use scenarios. There are issues with these comparisons. For example:

- the Waimakariri near-coastal mean flow (at the Old Highway Bridge gauge) is 119 m³/s, whereas the lower Rhine mean flow is 2900 m³/s;
- the Waimakariri mean annual flood at Old Highway Bridge is 1495 m³/s;
- most (77%) of the Waimakariri's suspended load is carried by flows between the mean and the mean annual flood, not around the mean flow (Hicks et al. 2018); and

- the flow of the lower Rhine (through the Netherlands, which was the focus of the Asselman et al. study) is highly regulated, particularly by upstream lakes, whereas the Waimakariri flow is not.

However, the main problem with the use of the Rhine figures is captured in the following extract from Asselman et al. (2000), page 48:

“For the Rhine basin downstream of the Alps, a decrease of sediment supply is predicted, at least for the lower (-16 %) and central estimates (-11 %) of climate change. For the upper estimate of climate change an increase of 8 % is calculated. For the Alps, the model results indicate that erosion and sediment supply will increase significantly. This effect of environmental change is likely to occur. However, the application of the sediment supply model to steep mountainous areas is rather dangerous and the results, thus, are probably unreliable. The sediment supplied in the Alps is trapped in the many large lakes at the foot of the Alps in Switzerland. This sediment is not available for transport to the Dutch waters. Therefore, the modelling results for the Alps are left out of consideration in the final figures that describe the effects of environmental change on erosion and sediment supply.”

In other words, the Asselman et al. figures on projected change in sediment load for the lower Rhine exclude projected climate-change driven sediment yield increases in the alpine headwaters region, and so provide no useful model for the Waimakariri. Indeed, the alpine headwaters of the Rhine should provide a better model.

Tonkin & Taylor (2017) chose not to consider the effects of projected increased rainfalls on coastal sediment supply because of a perceived long time-lag in the delivery of sediment from sites of accelerated erosion to the coast. However, this stems from references to experiences with gravel delivery to the coast, not fine sand being delivered primarily as suspended load – which is the situation with the Waimakariri (Hicks et al. 2018). As demonstrated in Section 3.3.4 of this report, the expected time-lag in delivering increased supplies of fine sand to the coast after a landslide in the Waimakariri Gorge amounts to only one-two years. Thus, even for climate-change driven accelerated erosion confined to the Waimakariri Catchment headwaters near the main divide (associated with more intense NW rainstorms), we should expect a latency of no more than a decade (and probably only a few years) before a signal appears in the coastal sand delivery. On that basis, the effects of intensifying rainfall should certainly be included in the future coastal sand budget.

Tonkin & Taylor’s projected decreases in Waimakariri sediment loads also appear to reflect expectations of sediment losses during water abstraction and gravel extraction operations on the Canterbury Plains. As we have discussed above, these effects are likely to be minor and well within the uncertainty around change in catchment erosion rates.

3.1.9 Summary of climate change effects on coastal sand delivery

In summary, projections of the effects of climate change on coastal sand delivery from the Waimakariri River are:

- A more-likely-than-not increase in sand delivery to the Canterbury Plains reach of the Waimakariri associated with intensifying and possibly increased rainfall in the catchment headwaters, particularly under the high emissions RCP8.5 scenario. Under that scenario, projected increases in sediment load by 2100 align bluntly, with an increase of more than 17% indicated from a simple assessment of projected

catchment rainfall and an increase of 28% indicated by the coupled climate and hydrological modelling. Since each assessment approach has its limitations, we cannot favour one over the other; however, we suggest using the coupled-modelling based figure (28%) as an upper bound because the rainfall based figure (17%+) remains semi-quantitative. However, there is large uncertainty with all these estimates of future river sand load, and the change could even involve a small decrease (of 8% or less as indicated by the coupled modelling) under a low emissions scenario.

- Associated changes in land cover are unlikely to have any significant effect.
- Any increased rates of gravel extraction from the Waimakariri channel will have negligible impact on sand delivery to the coast. Increased flood-harvesting from the lower Waimakariri River for irrigation water storage could reduce sand delivery to the coast by up to 3% if none of the diverted sand is returned to the river.

Little time-lag is anticipated between the effects of increased upper catchment rainfall on erosion and increased sand delivery to the coast. As determined in Section 3.3.4, the travel-time of sand load increases from the upper catchment should be around one to ten years at most.

3.2 Effects of wave climate change and sea-level rise

3.2.1 Changes to nearshore waves and longshore transport potential

Results from the SWAN modelling of the future scenarios listed in Table 2-2 are plotted in Figure 3-7. A commentary interpreting these results is provided in Table 3-3, with implications for the City shore summarised in the last column.

We are particularly interested in the effects on the net longshore transport potential, since this affects the southwards dispersion of the Waimakariri River sand along the City shore. Examining the changes in the northward and southward transport components informs on whether changes in the net drift are driven by changes in the north-easterly or southerly waves (or both). The southwards to gross transport ratio around the Waimakariri River mouth informs on the proportion of the river's sand load that is transported south onto the City shore. The divergence in the net longshore transport indicates the locations and extent of erosion or accretion associated with alongshore transport gradients.

Key results are:

- The 1.36 m sea-level rise scenario results in increased wave energy flux and consequently increased longshore transport potential. The increased onshore wave energy can be related to reduced bottom friction with deeper water, and this appears to be the main factor behind the increases in longshore transport potential. An increased ratio of southwards to gross longshore transport occurs around the river mouth (72% compared with 68% under the Baseline), indicating more of the Waimakariri River's sand is transported southwards, which should result in slightly increased accretion on the City shore compared to the current situation.
- The A2 Scenario delivers less wave energy overall but particularly from the north-easterly quarter, resulting in up to 25% less southwards transport along the City shore where southwards transport is the dominant control on the net longshore

transport. The ratio of southwards to gross transport around the Waimakariri River mouth falls from 68% (under the Baseline) to 59%, which indicates less of the Waimakariri River sand being distributed to the City shore and more transported northward from the river mouth.

- The effects of the B2 Scenario are similar in pattern to the A2 Scenario but the changes from the Baseline are smaller. This also portends a smaller share of the Waimakariri River sand for the City shore (61% southwards to gross drift ratio around river mouth), but the reduction is not as large as with the A2 Scenario.
- Including sea-level rise with the A2 and B2 Scenarios still reduces the proportion of river sand distributed southward to the City shore compared to the Baseline situation (to 64% for the A2-SLR combination and to 66% for the B2-SLR combination), but the net change from the Baseline is smaller than when just considering the effects of these wave scenarios on their own.
- Since the high sea-level rise scenario and the A2 wave scenario are both aligned with the high emissions (RCP8.5) climate change scenario, their combination likely indicates a maximum reduction in the proportion of the Waimakariri River sand that is moved south (that is, future P_s values in Equations 5 and 6 could fall to no less than 64% by the end of the century, compared to the current 68% value).

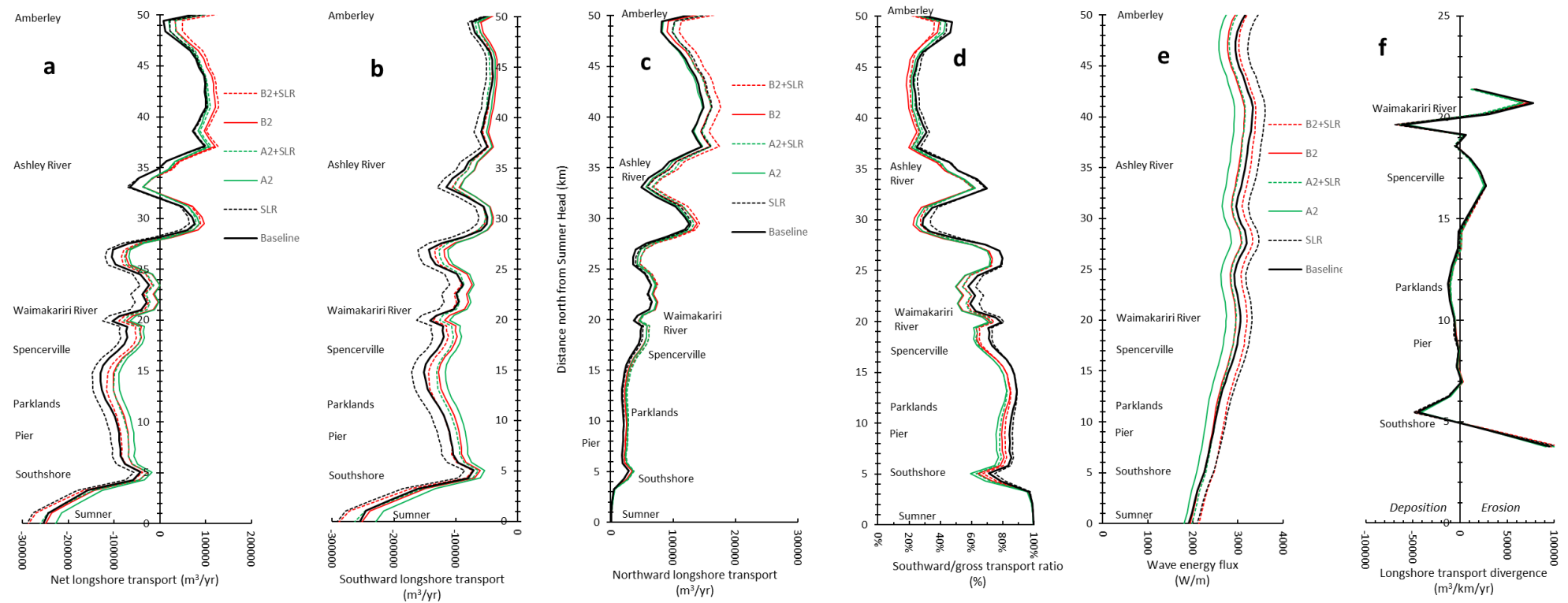


Figure 3-7: Wave energy and longshore transport potential along Pegasus Bay under different climate change and sea-level rise scenarios. (a) Net longshore transport potential (northward transport is positive, southward transport is negative). (b) Southward longshore transport potential. (c) northward longshore transport potential. (d) ratio of southward to gross longshore transport potential (gross transport = sum of southward and northward transport). (e) Wave energy flux at present 10 m bathymetry contour. (f) Longshore transport potential divergence (positive indicates erosion, negative indicates deposition). Scenarios (Baseline, SLR, A2, B2, A2 + SLR, and B2 +SLR) defined in Table 2-2.

Table 3-3: Commentary on changes (from Baseline) in wave energy and longshore transport patterns under climate-change and sea-level rise scenarios. Based on data plotted in Figure 3-7. Scenarios defined in Table 2 2.

Scenario	Southward transport	Northward transport	Net longshore transport	Southward to gross transport ratio	Wave energy flux	Longshore transport divergence	Key signals for City shore
SLR (1.36 m)	10% increase along the whole Pegasus Bay shore.	Few % increase along Pegasus Bay shore.	Increased net drift all along bay, with greater increase towards southern end of bay.	Ratio increased by a few percent along most of bay; averages 72.4% around Waimakariri mouth ⁸ (c/f 68.2% under Baseline); suggests a small increase in proportion of Waimakariri River's sand yield that is transported south.	Increases by 8-10% all along the bay; due to reduced friction due to deeper water; appears to be main factor behind the increase in longshore transport potential.	No change in divergence pattern south of the Waimakariri, with only a very small increase in amplitude, indicating a very small increase in deposition rates due to transport gradients.	Small increase in sand deposition associated with larger share of river sand.
A2	Southwards transport reduced by ~ 20% along City shore; less reduction at northern end of bay.	Negligible change in northward transport.	Reduction in net transport most prominent along City shore due to less southward transport; reduction tapers to north. Signals reduced sand supply from river to city beaches.	Reduces along most of Pegasus Bay; averages 59.6% around Waimakariri mouth (c/f 68.2% under Baseline); signals less effective southwards transport and river sand dispersion to south.	Reduced all along Pegasus Bay, proportionally more so towards northern end.	Very small reduction in negative transport divergence along City shore, signalling small reduction in sand accretion.	Less effective southwards transport delivers less river sand.

⁸ The ratio of southwards drift to gross drift at the Waimakariri River mouth was spatially averaged across five SWAN output stations (Stations 72-76) spanning 2.65 km of shore centred at the river mouth.

Scenario	Southward transport	Northward transport	Net longshore transport	Southward to gross transport ratio	Wave energy flux	Longshore transport divergence	Key signals for City shore
A2 + SLR	Sea-level rise partially offsets reduction in southward transport along City shore due to Scenario A2.	Increases slightly due mainly to sea-level rise effects.	Sea-level rise only partially offsets reduction in southward net transport along City shore due to Scenario A2; slight increase in northward transport further reduces net southward transport along City shore.	Sea-level rise induces only a slight recovery in ratio, leaving a lower ratio compared with baseline; averages 63.7% around Waimakariri mouth (c/f 68.2% under Baseline); indicates less effective southward dispersion of river sand.	Sea-level rise effects substantially offset the reduction in wave energy associated with Scenario A2.	No significant difference in divergence pattern or amplitude.	Less effective southwards transport delivers less river sand, although slightly better with sea-level rise than without it.
B2	Southwards transport reduced by ~ 10% along City shore; less reduction at northern end of bay.	Few % increase along Pegasus Bay shore (of similar magnitude to that due to sea-level rise).	Reduced net southward transport along City shore; increased net northward transport along northern bay shore.	Reduces along most of Pegasus Bay; averages 60.9% around Waimakariri mouth (c/f 68.2% under Baseline); signals less effective southwards transport and river sand dispersion to south.	Very small reduction from around Spencerville north.	Minimal change.	Less effective southwards transport delivers less river sand; impact less than Scenario A2.

Scenario	Southward transport	Northward transport	Net longshore transport	Southward to gross transport ratio	Wave energy flux	Longshore transport divergence	Key signals for City shore
B2 + SLR	Sea-level rise largely offsets reduction in southward transport along City shore due to Scenario B2.	Increases by ~ 10-15% all along Pegasus Bay shore due to compounding effects of B2 and SLR.	Little net change along City shore due to compensating effects of sea-level rise and wave climate change on southward dominant transport; towards north of bay (where northward transport dominates), wave climate change and sea-level rise reinforce to increase net transport.	Reduction due to B2 Scenario partially offset by sea-level rise; averages 65.7% around Waimakariri mouth (c/f 68.2% under Baseline).	Effect of sea-level rise prevails over wave climate change, resulting in net increase in wave energy (by ~ 5-10%).	Minimal change.	Slightly less river sand delivered south due to increasing intensity of northwards transport.

3.2.2 Changes in closure depth

Estimated change in outer profile closure-depths from analysis of the SWAN model runs for the various sea-level rise and climate change scenarios are shown in Table 3-4. These are provided for three SWAN model output stations spanning the City shore (Southshore, Parklands, and Pines Beach), and cover a gradient of exposure to waves from the southerly quarter.

The profile closure depth may be selected as either the inner or outer of Hallermeier's depths (D_i and D_o) for effective wave disturbance, but in keeping with Hicks et al. (2018) we take the outer limit D_o to represent the closure depth.

At Southshore (where the sheltering from southerly waves is greatest), the 1.36 m sea-level rise scenario deepens D_o by 0.27 m, the A2 Scenario shallows D_o by 0.29 m, and the B2 Scenario shallows D_o slightly by 0.04 m. With the A2+SLR scenario, the amelioration of the deep-water wave climate associated with A2 offsets the effects of the 1.36 m rise in sea-level⁹, while with the B2+SLR scenario the effects of the sea-level rise largely prevail.

Very similar changes to D_o occur at the other stations under sea-level rise, but there appears to be a northwards trend for progressively greater shallowing of D_o under both Scenarios A2 and B2 -with the result being that off Pines Beach (at the northern end of the study shore) the shallowing of D_o under A2 more than offsets the deepening in D_o due to the sea-level rise (resulting in a net reduction in D_o by 0.39 m under the A2+SLR scenario), while the shallowing under B2 largely offsets the deepening due to sea-level rise (resulting in little net change under the B2+SLR scenario).

The changes in D_i associated with the various scenarios (Table 3-4) match those for D_o but are approximately 2/3 the magnitude (due to the 1.5 factor used to convert D_i to D_o u).

Summary and implications for sand volume needs to offset sea-level rise

In summary, this analysis indicates two counter-balancing effects of climate change on closure depth: (i) sea-level rise will increase the closure depth by enabling high waves to propagate shoreward with less energy dissipation (therefore "stirring-up" seabed sediment at greater water depths); (ii) high waves will occur a little less often under the more extreme (higher emissions) climate change scenarios, thus reducing the closure depth slightly. Which effect prevails depends on the scenarios chosen and the location along the shore. Since the sea-level-rise and wave-climate scenarios investigated here align with the more extreme (high emissions) RCP scenarios, then they likely provide upper-bounds for what will eventuate. In this context, and because the changes in closure depth associated with the modelled scenarios are all relatively small (of the order of 0.65 m or less) compared with the uncertainty in what the actual current closure depth is (i.e., the inner and outer depth limits differ by 2.0-2.3 m under the Baseline Scenario), then these effects are expected to have only minor impact on the sand demand to counter a rising sea-level in the shore sand budget.

⁹ We observe from Table 3-4 that the change in closure depth associated with the A2+SLR scenario is much the same as the algebraic sum of the changes due to the A2 and SLR scenarios (and similarly with the B2+SLR Scenario). This means that to a reasonable approximation, at least for assessing closure depth, it is not necessary to repeat SWAN runs for sea-level rise and wave climate combinations.

Table 3-4: Inner and outer profile closure depth estimates at Southshore, Parklands, and Pines Beach wave output stations for climate change and sea-level rise scenarios. Based on SWAN modelling 2000 through 2017. Scenarios defined in Table 2 2. H_{s-e} is the effective significant wave height; T_{s-e} is the matching average peak-energy wave period; H_{s-max} is the maximum significant wave height in the record; D_i is the inner closure depth limit and D_o is the outer limit, as defined in Hicks et al. (2018). Both D_i and D_o have been adjusted to MSL datum by adding 1.0 m.

SWAN output station	Scenario	H_{s-e} (m)	H_{s-max} (m)	T_{s-e} (s)	D_i (m)	D_o (m)	Change from Baseline D_i (m)	Change from Baseline D_o (m)
Southshore (Stn 50)	Baseline	1.91	3.44	7.56	4.91	6.86	NA	NA
	SLR	1.99	3.72	7.86	5.09	7.13	0.18	0.27
	A2	1.85	3.19	6.90	4.72	6.57	-0.19	-0.29
	A2+SLR	1.92	3.41	7.15	4.87	6.81	-0.03	-0.05
	B2	1.92	3.26	7.22	4.88	6.83	-0.02	-0.04
	B2+SLR	1.99	3.50	7.48	5.04	7.07	0.13	0.20
Parklands (Stn 61)	Baseline	2.06	3.77	7.99	5.23	7.35	NA	NA
	SLR	2.14	4.15	8.35	5.42	7.63	0.19	0.28
	A2	1.92	3.53	6.98	4.85	6.77	-0.38	-0.57
	A2+SLR	1.99	3.77	7.25	5.01	7.02	-0.22	-0.33
	B2	2.01	3.60	7.44	5.07	7.11	-0.16	-0.24
	B2+SLR	2.09	3.86	7.70	5.25	7.38	0.02	0.03
Pines Beach (Stn 75)	Baseline	2.25	3.88	7.98	5.57	7.86	NA	NA
	SLR	2.32	4.31	8.46	5.76	8.15	0.19	0.28
	A2	2.05	3.78	7.42	5.14	7.21	-0.43	-0.65
	A2+SLR	2.12	4.08	7.76	5.31	7.47	-0.26	-0.39
	B2	2.15	3.83	7.61	5.34	7.52	-0.23	-0.35
	B2+SLR	2.22	4.16	8.03	5.53	7.79	-0.05	-0.07

3.2.3 Avon-Heathcote Estuary tidal prism and sand entrapment

A digital elevation model (DEM) of the general area of the Avon-Heathcote ebb-delta generated from the 1996 bathymetric survey data is shown in Figure 3-8A. Figure 3-8B shows a “no delta” DEM produced by interpolating contours across the delta.

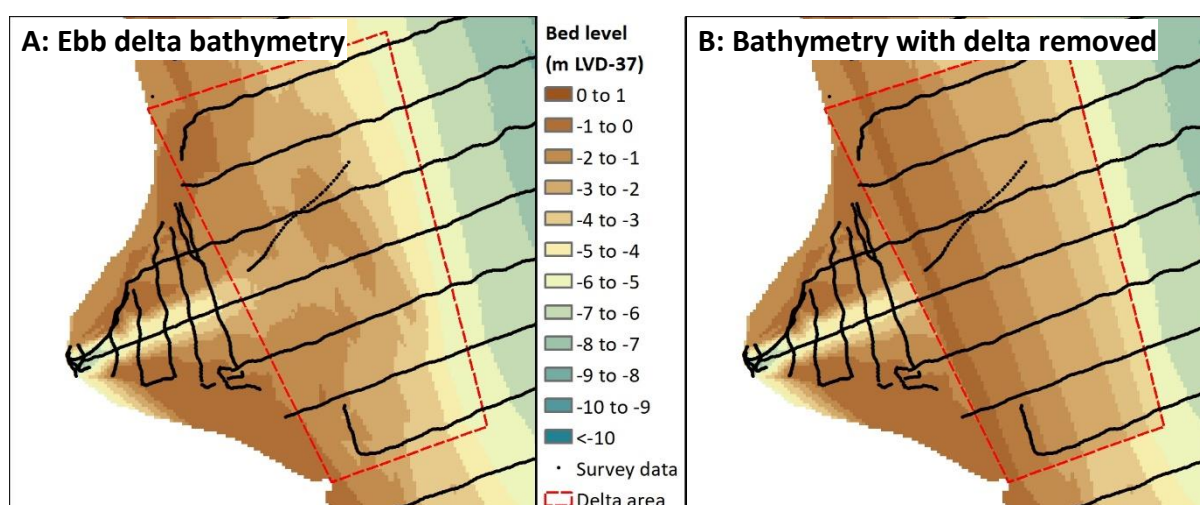


Figure 3-8: Avon-Heathcote Estuary ebb-delta bathymetry. A: bathymetry as interpolated from 1996 survey data. B: bathymetry replaced with interpolated data in the identified delta area.

The ebb-delta volume calculated by differencing the actual and ‘no delta’ DEMs was 250,000 m³. The sparse survey data and location of the estuary mouth at a point of changing shoreline orientation made identification of the delta extent and interpolation of the no-delta bathymetry challenging. For these reasons it is quite likely that the delta could extend further offshore and alongshore than identified, meaning that this volume estimate should be considered a lower bound.

The spring-tide tidal-prism volume of the estuary under pre-earthquake, current, and sea-level rise conditions was simulated using the Delft3D hydrodynamic model of the estuary (Measures and Bind 2013). The calculated tidal-prism volumes are shown in Table 3-5.

Table 3-5: Avon-Heathcote Estuary Ihutai spring-tide tidal-prism volume and throat cross-section area. Tidal prism volume calculated from Delft3D hydrodynamic model simulations of the estuary. Throat area estimated from empirical relationship with tidal prism volume.

Estuary bathymetry	Sea-level	Spring tidal prism (m ³)	Tidal prism difference from present	Inlet throat area (m ²)	Throat area difference from present (m ² and %)
Pre-earthquake	Present SL	12,000,000	+15%	730	97 (15%)
Post-earthquake	Present SL	10,400,000	NA	633	NA
Post-earthquake	0.5 m SLR	14,700,000	+40%	895	262 (41%)
Post-earthquake	1.0 m SLR	18,500,000	+77%	1,126	493 (78%)

Based on the modelled tidal prism volumes it is possible to estimate the volume of sand retained in the ebb-tidal delta under the different modelled scenarios. Ebb-delta volume estimates were calculated from the Hicks and Hume (1996) relationship (labelled “uncalibrated” in Table 3-6), as well as after calibrating this relationship based on the measured lower bound pre-earthquake ebb-delta volume (labelled “lower bound” in Table 3-6). The calibration influences the overall magnitude of the ebb-delta volume by almost one order of magnitude but has no effect on the relative delta volume under the different scenarios.

Table 3-6: Estimated ebb-delta and inlet throat sand volume changes after Christchurch Earthquake and sea-level rise.

Scenario	Estimated ebb-delta volume		Difference to present ebb-delta volume			Throat volume difference
	Uncalibrated (m ³)	Lower bound (m ³)	Uncalibrated (m ³)	Lower bound (m ³)	% Change	(m ³)
Pre-earthquake	1,800,000	250,000	320,000	40,000	22%	93,000
Present	1,480,000	210,000	0	0	0%	0
0.5 m SLR	2,390,000	330,000	910,000	130,000	61%	157,000
1.0 m SLR	3,310,000	460,000	1,830,000	250,000	124%	296,000

The larger ebb delta sizes in Table 3-6 with sea-level rise require stocking from a local sand source. The two available sources are the adjacent beaches and the tidal inlet throat, which is also expected to enlarge with an increased tidal prism. The throat area changes (predicted with Equation 3 and listed in Table 3-5) indicate volumes of 157,000 m³ and 296,000 m³ for 0.5 and 1.0 m rises in sea-level, respectively (Table 3-6).

These throat volumes roughly balance the “lower bound” ebb-delta sand demand estimate, so in that case there would be no need for additional sand from the adjacent beaches. Assuming a 100-year time frame with the “uncalibrated” ebb-delta volume estimates, the residual sand deficits from the adjacent beaches with a 0.5 m sea-level rise would create a sand demand averaging 7,500 m³/yr, while a 1.0 m rise would require 15,300 m³/yr of sand.

Thus, the ebb-delta sand demand with rising sea-level could range between zero and 15,300 m³/yr. This equates to zero to 8% of the current (182,000 m³/yr) river sand supply rate to the City shore, which is well within the uncertainty of the river sand supply rate and the potential future changes to it. On that basis, and because of the considerable uncertainty on the true extent of the ebb-delta, we have ignored this term in the sand budgeting undertaken in Section 3.4.

3.2.4 Effects on shore stability at the Avon-Heathcote inlet

As discussed above, the increased tidal prism of the Avon-Heathcote Estuary under a higher sea-level is expected to increase the cross-section area of the inlet throat by 41% for a 0.5 m sea-level rise and by 78% for a 1.0 m rise (Table 3-5). Assuming that this increase will be taken-up equally by an increase in average channel depth and width, the indicated increases in width would be 19% and 33%, respectively. Since the inlet’s southern bank is fixed in location by rocky outcrops, then the width increase would be accommodated by erosion of the tip of the Southshore Spit. Thus, at the throat’s current narrowest point which is 200 m wide, the Southshore Spit would retreat by 38-66 m.

We note, though, that this retreat would be a long-term average response and is small compared to the scale of spit tip advances and retreats (several hundred metres over multi-year time scales) that have been recorded historically (Allan et al. 1999). These large-scale shore excursions are associated with changes in the form of the ebb-delta and tidal channels, often forced suddenly by large wave events or driven progressively by onshore-migrating sand bars. Such large-scale shore movements at the spit tip area should continue to prevail in the future, and their zone of influence will likely extend further north as the tidal system energy increases with growing tidal prisms.

3.3 Potential effects of a major earthquake on the Waimakariri River sand delivery

3.3.1 Landslide locations, volumes, and grainsize

Potential locations vulnerable to large landslides in the event of a major earthquake on the Alpine Fault, or other major faults (such as the Porters Pass Fault in the Waimakariri Gorge or the Esk Fault) were identified by inspecting maps and aerial imagery. Six indicative major landslides were identified as shown in Figure 3-9, Figure 3-10, and Table 3-7. The volume of each landslide ranged from 10 to 150 million m³, and the cumulative volume of all six landslides was approximately 300 million m³.

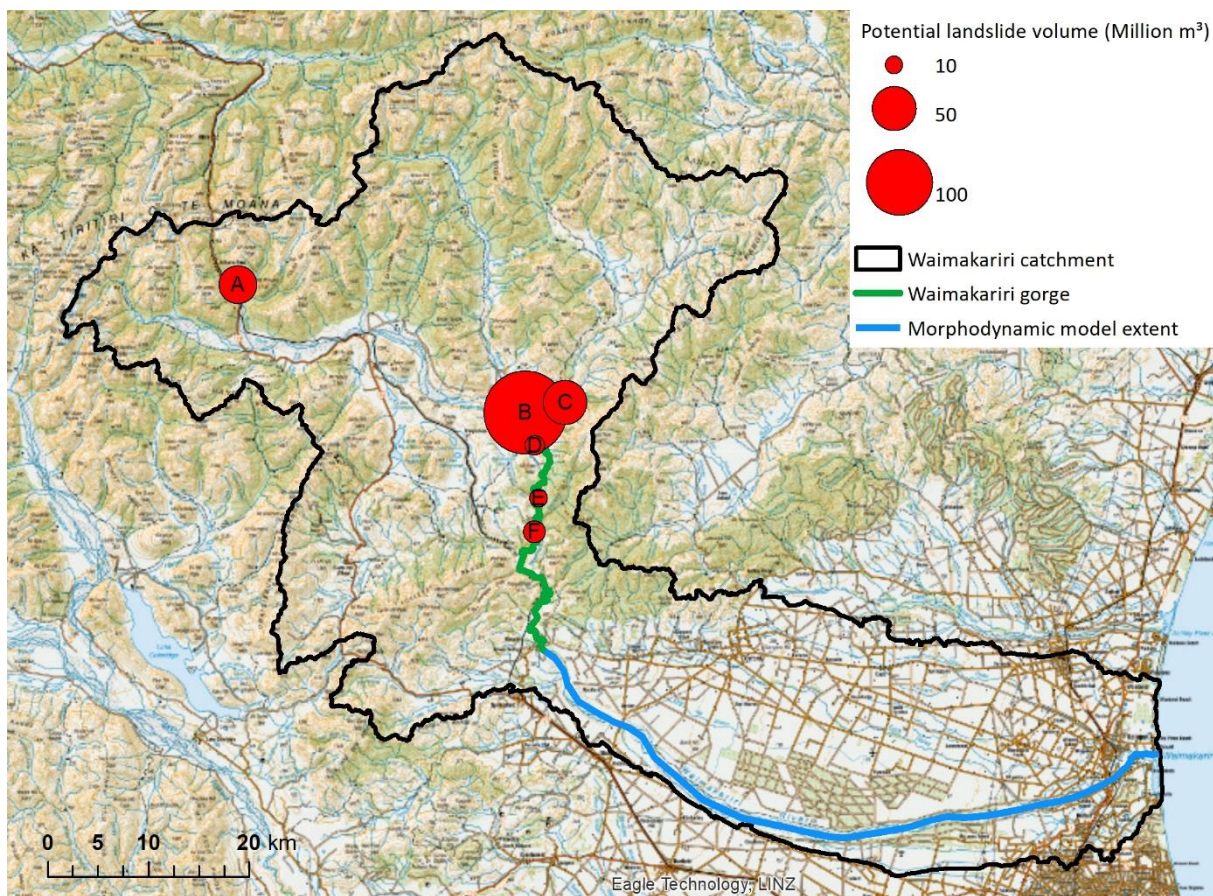


Figure 3-9: Location of six indicative potential major landslides in Waimakariri Catchment. Landslide locations shown in relation to Waimakariri Gorge and the morphological model extent. Landslides are marked by red circles with size proportional to potential landslide volume. Letters correspond to landslide details in Table 3-7 and Google Earth images in Figure 3-10.

Table 3-7: Location and size of six indicative major earthquake induced landslides in the Waimakariri Catchment. Letters correspond to landslide locations shown in Figure 3-9 and Google Earth images in Figure 3-10.

	Landslide location	Landslide size (Million m ³)
A	SW-face of Mt O'Malley collapse into left bank of Bealey River	50
B	SW face of Whale Hill collapse into left bank of Waimakariri just upstream of gorge	150
C	Terrace slump into right bank of Esk River 3.6 km upstream of Waimakariri confluence	50
D	Terrace slump into right bank of Waimakariri Gorge immediately downstream of Esk confluence	12.5
E	Gully expansion on left bank of Waimakariri Gorge	15
F	Hillside slump into right bank of Waimakariri Gorge	10

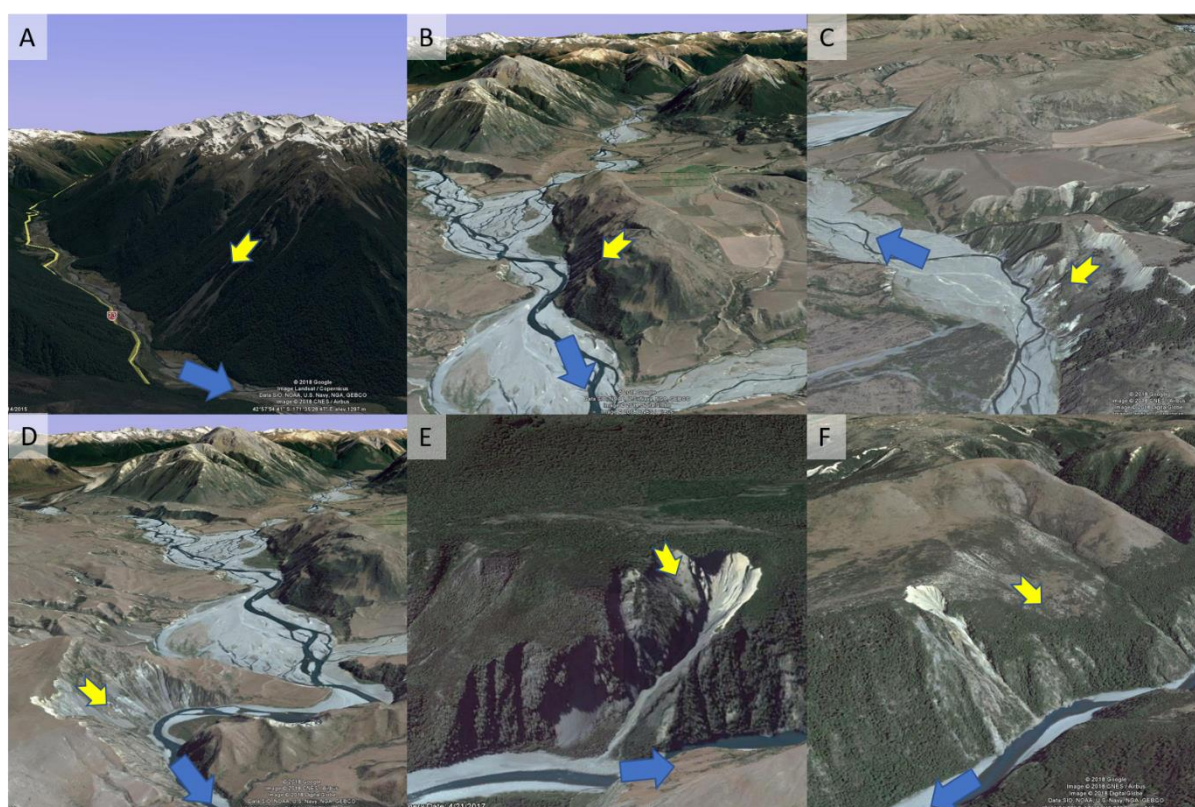


Figure 3-10: Google Earth images of indicative major landslides. Letters correspond to landslide locations shown in Figure 3-9 and landslides details in Table 3-7.

McSaveney and Davies (2007) discuss the grainsize distribution of landslides and provide several example distributions from significant New Zealand landslides (Figure 3-11). Some of the examples plotted are within or very close to the Waimakariri Catchment and/or have similar geology. An assumed landslide grainsize distribution (shown in Figure 3-11) was developed for the modelling based on the observed distributions from the Mt Cook, Coleridge, Craigieburn, Falling Mountain, and

Acheron landslides. The proportion of total landslide volume which consists of sand ranges from 7% (Acheron) to 25% (Craigieburn and Coleridge) with the assumed distribution consisting of 20% sand.

3.3.2 Landslide sediment entrainment into the river

Croissant et al. (2017) show that half of a landslide's volume is typically removed in 5 to 25 years and that modification of river width plays a key role in speeding-up evacuation of landslide material. They investigated the combined effect of multiple landslides under different hydraulic conditions and, for the case of the Southern Alps of New Zealand, found that half the total landslide volume would likely be eroded in 4.4 to 8.5 years for earthquake magnitudes between 7 and 9. Based on this study we assumed that half the landslide volume would enter the river system within 6.5 years of an earthquake, with the delivery declining exponentially with time.

3.3.3 Effects of landslide dams

Of the potential landslides identified, we analysed the potential for lakes to be generated by landslides B and D (see Figure 3-10 and Table 3-7). These locations were selected as they are the most likely to cause large lakes (i.e., both are at relatively narrow cross-sections with large river flats upstream). Locations E and F are also at narrow cross-sections which could be blocked, but are unlikely to impound substantial lakes due to the narrow river gorge upstream of them. For landslides B and D, we considered three dam heights: 50 m, representing an upper bound estimate of the initial dam size; 25 m, representing a smaller initial dam; and 10 m, representing the residual dam after significant erosion. We calculated the time for the lakes to fill at median river flow (Table 3-8).

Table 3-8: Estimated landslide dam lake volumes and fill times. Dam locations shown in Figure 3-10.

Dam location	Valley width (m)*	Dam height (m)	Lake Volume (million m ³)	Lake Area (km ²)	Time to fill (days)
B (Whale Hill)	300 - 600	50	417	18.3	57
		25	106	8.3	15
		10	25	4.6	3
D (Upstream end of gorge)	200 - 400	50	388	16.3	53
		25	93	8.5	13
		10	23	2.4	3

* A range of valley width is given as it depends on exact location of dam.

The larger (25-m and 50-m high) dams would impound substantial water volumes, taking up to two months to fill at median flow (but it is likely that the lakes would fill faster if a flood occurred within this period). After filling and spilling, we consider the dam crests would be substantially lowered, if not completely removed, by erosion during subsequent floods. We consider this would occur rapidly because of (i) the frequent large floods which occur in the Waimakariri (mean annual flood is ~ 1300 m³/s), and (ii) landslide dams in the greywacke/argillite terrane of the Waimakariri catchment are not expected to contain large proportions of very coarse sediment that would armour channels (as indicated by Figure 3-11). Thus, under this lake-filling then rapid down-cutting scenario, the delay before the onset of the type of response modelled by Croissant et al. (2017) would amount to a few months at most.

If the landslide dams were not completely removed, we consider it likely that the residual dams would be at most 10-m high. These, however, would still impound 23-25 million m³ lakes which

would create efficient sediment traps for sand and coarser sediment. The amount of sediment which these dams could impound could potentially be over 25 million m³ (allowing for a sloping bed surface which would form behind the dam), but this is likely to be much less than the estimated 300 million m³ of sediment entering the river system from all landslides as a result of the earthquake.

In summary, while it is possible for landslide dams to impound sediment and reduce sediment supply, we consider this effect is likely to be dwarfed by the increased supply resulting from a large earthquake causing multiple landslides.

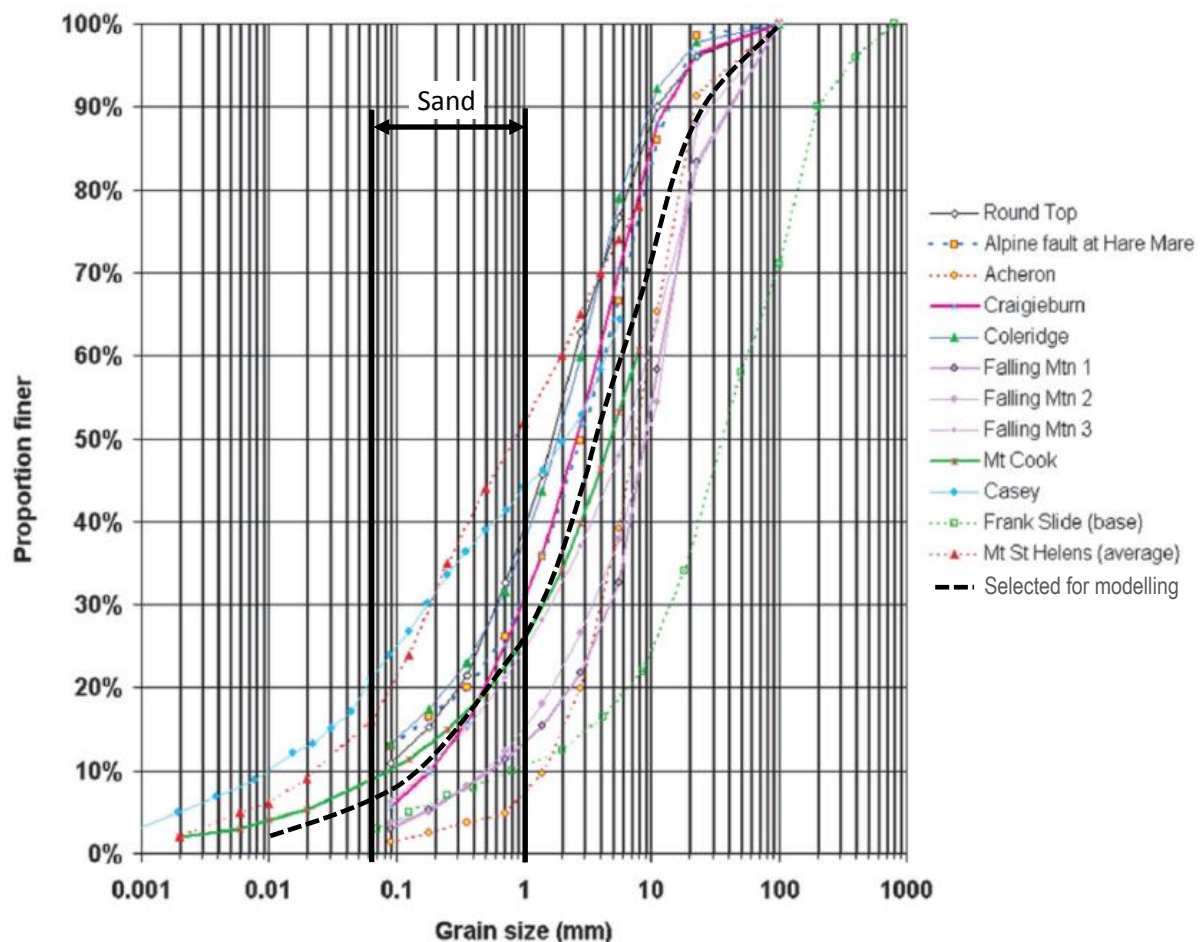


Figure 3-11: Landslide grainsize distribution selected for modelling compared to measured grainsize distributions of a number of landslide deposits. Measured distributions reproduced from Figure 8.5 of McSaveney and Davies (2007). Thicker black vertical lines indicate the limits of sand sized sediment. Note that the Alpine Fault and Casey are samples of fault-gouge rather than landslide deposits.

3.3.4 Sediment transfer to the coast

Based on the indicative total landslide volume (300 million m³), time taken for 50% of the landslide material to enter the river system (6.5 years), and the proportion of sand sized material (20%), we estimate the rate of sand delivery into the river system as shown in Figure 3-12. This additional sand input was used as the basis for morphological modelling of sediment transport in the Lower Waimakariri River following a major earthquake as described in Section 2.3. Modelling was carried out with and without the additional landslide input to be able to isolate the effect of the landslides.

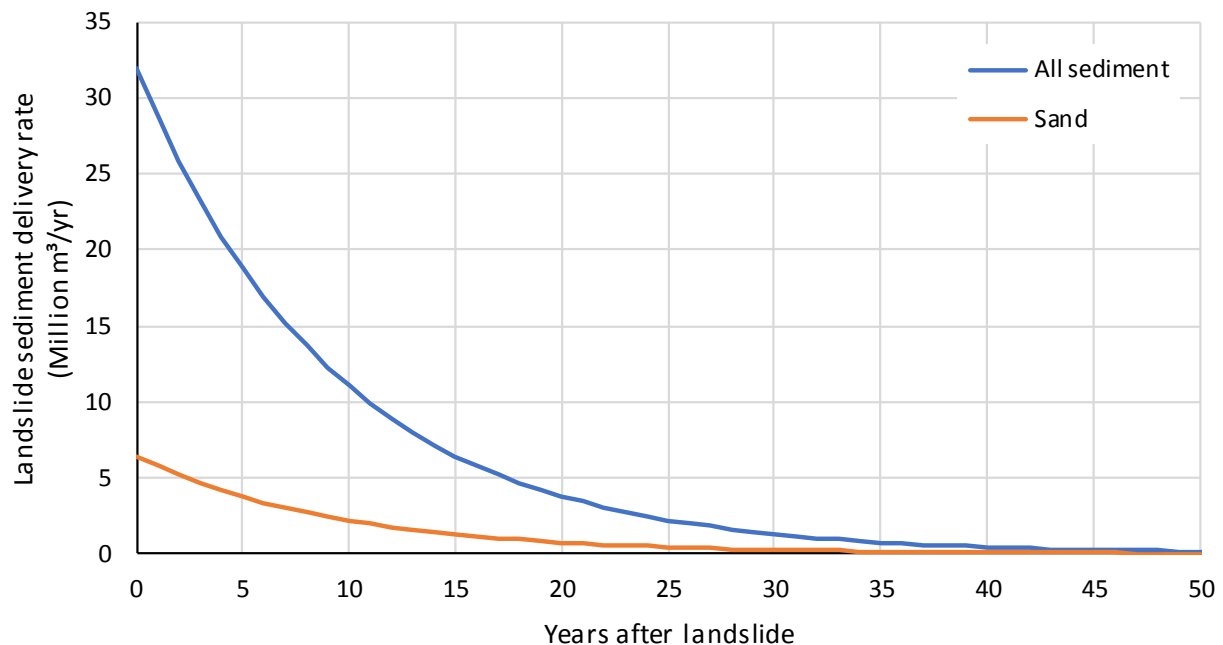


Figure 3-12: Estimated rate of delivery of all sediment and sand into the Waimakariri River system from earthquake induced landslides.

Figure 3-13 shows the sand delivery to the coast with and without additional landslide inputs. Key results are:

- Landslide derived sand delivery to the coast peaks approximately five years after landslides/earthquake occurrence.
- Landslides cause the river's coastal sand delivery to more than double for about 10 years.
- Half of the landslide-sourced sand that is delivered to the coast is delivered in 11 years, with 90% in 30 years.
- The modelling was uncalibrated and approximately 30% of the 1.19 million t/yr (0.75 million m³/yr) baseline sand load was deposited in the model. We do not expect such sand deposition would actually be so extensive (based on the absence of substantial sand deposits on the current Lower Waimakariri braidplain). To correct for this, model results at the coast (both baseline and landslide) could be scaled-up.
- In excess of 50% of the landslide derived sand is trapped within the bed of the model in aggrading reaches. Whilst this is likely a real effect, size gradings of bed material samples from the lower, braided reach of the Waimakariri show that sand makes up only a small proportion of the bed material. For this reason, it seems likely that the model is trapping more sand than would occur in reality, so the model likely underestimates sand delivery to the coast – potentially by near a factor-of-two.

While we have confidence around the model-indicated time-scales of landslide sand delivery, the last two points, along with the uncertainties around what landslides might actually occur during an alpine earthquake and potential sediment retention behind dams, caution that the volumes of landslide sand delivered to the coast should be regarded as “indicative” only.

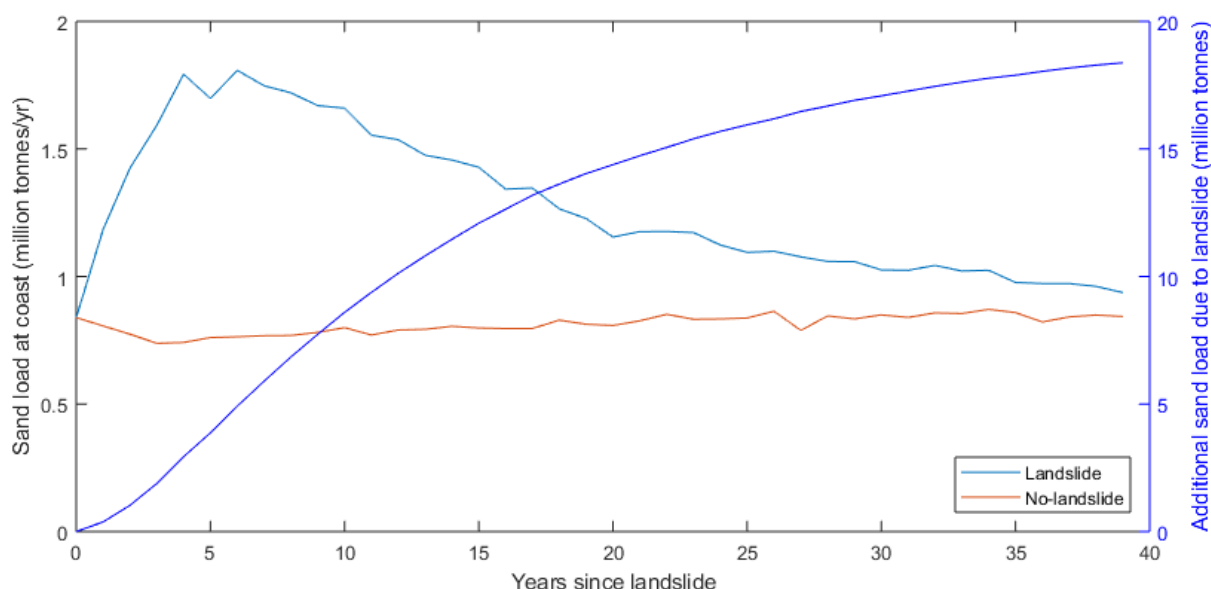


Figure 3-13: Modelled coastal sand delivery with and without earthquake induced landslide activity. Blue curve shows the cumulative coastal delivery of landslide-sourced sand with time. Note that inter-annual variability in sediment load associated with hydrological variability has been removed by running simulations with an average hydrograph derived from long-term average flow-duration curve.

The model also shows that while sand moves rapidly through the system, primarily as suspended load, gravel travels as a dispersing aggradational wave that moves much more slowly. This is consistent with previous morphological modelling of gravel transport in the Waimakariri which showed that 45 years after an earthquake-induced increase in gravel supply, increased transport of gravelly bedload had only propagated 16 km into the model (Measures 2012). Given that this increased transport is accompanied by significant bed aggradation which would increase flood risk, and that gravel demand in the Waimakariri currently exceeds supply, it is anticipated that gravel extraction would be increased to manage increased gravel delivery (pers. comm. Shaun McCracken, Environment Canterbury 2018).

The magnitude and time-scale of the sediment delivery predicted by the modelling was “sensitivity checked” based on published analysis of sediment delivery from previous earthquakes.

Analysis of field investigations by Wells and Goff (2007) show that tectonic activity associated with the Alpine Fault is the primary controlling influence forming shore-parallel dune ridge sequences in South Westland. Evidence from tree ring dating shows that significant coastal progradation started within 5-11 years of major earthquakes. Goff et al. (2008) provided further evidence of seismic events in New Zealand producing short lived river sand supply pulses linked with discrete phases of coastal dune building.

McFadgen and Goff (2005) investigated the role of earthquake activity in influencing the Avon-Heathcote Estuary by dating of sediment deposits. They linked periods of dune development in Pegasus Bay to earthquake activity and concluded that dune development occurs soon after tectonic activity, while river channel avulsion (i.e., the river switching its pathway across its alluvial fan, e.g., from discharging north into Pegasus Bay to discharging south into Te Waihora) relates to periods of tectonic activity that occurred 100–200 years previously.

This evidence matches the timing of the modelled sediment delivery reasonably well in that fine sediment arrives at the coast relatively rapidly following an earthquake with the effects of gravel delivery taking longer. We could find no studies which looked at the volumes of sediment delivery by the Waimakariri River associated with particular historic earthquakes.

3.3.5 Landslide sand transfer along the coast

While there would be little time-lag between the earthquake and the boosted sand delivery to the coast, there would be a longer time before coastal processes spread the sand pulse along the city shore. Hicks et al. (2018, their Figure 3-15) identified from the ECan beach profile dataset a possible sand wave migrating southward from the Waimakariri River mouth at a rate of about 330 m/yr. Similar (albeit slightly faster) rates of sand dispersion alongshore from river mouths following large deliveries of river sand have been reported in the literature. For example, Hicks and Inman (1987) observed a dispersing sand wave migrating downdrift¹⁰ from the San Lorenzo River (California) at 500-750 m/yr following a large river flood, while the data of Gelfenbaum et al. (2015) show a sand pulse migrating at about 1250 m/yr alongshore from the mouth of the Elwha River following dam removal on the Elwha River (Washington State, USA). At these rates, it could require one to several decades for a sand pulse to reach Waimairi Beach and longer for it to reach Southshore. During the process, the sand pulse would almost certainly diffuse in amplitude as well.

In both the San Lorenzo and Elwha River examples, the alongshore dispersion of the river sand was delayed by some months before sand was moved onshore from the river delta. The beginning of landslide sand movement onshore at the Waimakariri River mouth would involve a similar time lag following the first flood after the earthquake. These other river examples also showed that once deposited at the river mouth, the sand was merged into the littoral system and transported alongshore by coastal processes and events disconnected from river events. We would expect similar river/coastal process de-coupling in the Waimakariri case. This is discussed further in Section 3.5.

3.4 Effects of future sand budget changes on sand volumes and shoreline position

3.4.1 Summary of potential sand budget changes

Summarising the findings of the sections above:

- Changes to delivery of Waimakariri River sand to the coast¹¹ over the next 100 years:
 - The regional climate-change documentation suggested a likely increase of around 17% due to intensifying rainfall in the Waimakariri headwaters.

¹⁰ The term “downdrift” refers to the direction of prevailing longshore transport (which is often referred to as “littoral drift”).

¹¹ The current river sand load to the coast was estimated by Hicks et al. (2018) as 745,000 m³/yr (Figure 1-1).

- The Kidson weather type analysis suggested possibly fewer NW rainstorms (less catchment erosion) but this will likely be offset by more intense storms (more catchment erosion), so the net direction of change for sediment loading is unclear.
- The coupled climate and hydrological modelling of the Waimakariri River flows suggested the river sediment loads by 2100 could range from 8% less than at present (RCP4.5 Scenario) to 28% more (RCP8.5 Scenario).
- Increased future irrigation water demand could potentially increase the “collateral” sand loss from the river by the equivalent of about 3% of the current sand load – if this intercepted sand is not returned to the river.
- Future gravel extraction from the river channel should have no net impact on the river’s sand delivery, since sand taken with extracted gravel would otherwise remain bound in the river bed.
- Thus potentially, the river’s sand delivery to the tidal reach could vary between a reduction of 11% (8% reduction from up-catchment and 3% interception by irrigation takes, with no sand returns to the river) and a 28% increase (28% increase from up-catchment and all irrigation-intercepted sand flushed back to the river).
- Sea-level rise driven deposition in the tidal reach of the Waimakariri River would be 1,300 m³/yr under the status quo (sea-level rise rate of 2 mm/yr), 3,600 m³/yr with a rise-rate of 5.4 mm/yr, and 8,800 m³/yr with a rise-rate of 11 mm/yr.
- Possible additional sand load associated with a major alpine earthquake:
 - Following a major future alpine earthquake (which could occur in the next century), landslides (we estimate a 300 million m³ combined volume of which 20% renders to sand) clustering mainly in or just upstream of the Waimakariri Gorge could at least double (possibly treble) the river’s sand load for over 10 years, with landslide sand first arriving at the coast within 1-2 years of the landslide event, and 90% of the landslides’ coastal sand delivery occurring over 30 years. Dispersion of the landslide’s sand pulse along the shore by coastal processes would likely occur slowly, with one to several decades elapsing before any signature appeared at Waimairi Beach and longer to reach Southshore. While there is considerable uncertainty over what the net additional volume of sand delivered to the coast would be, there is greater certainty in the response times.
- Trap efficiency of river sand on the beach profile:
 - The trap efficiency refers to the likelihood that a river sediment grain of given size will be retained on the beach profile above the closure depth, rather than being dispersed offshore while suspended in currents or by diffusion processes. Mud grains, for example, are not found on the Pegasus Bay beaches because they are too easily suspended by waves and currents, thus they have a trap efficiency of zero. Hicks et al. (2018) determined trap-efficiencies for the range of grainsizes comprising the Waimakariri River sediment load by matching the river load size grading with that of the beach sediment, which indicated an overall river sand

trap efficiency (load-weighted over all sand grades) of 36%, albeit with some uncertainty. We use the same value for this study, assuming that the future river sediment load size grading will not change and that the sediment resuspension capability of future nearshore current and wave regimes will not change appreciably (the latter assumption was verified by our analysis of closure-depth change, which showed only relatively small changes in closure depth under the “high emissions” A2 wave-climate scenario).

- Proportion of river sand load transported south towards the City shore:
 - Indexed by the ratio of southward longshore transport potential to gross longshore transport potential about the Waimakariri River mouth, the proportion of river sand transported south ranges from 72.4% after a sea-level rise of 1.36 m to 59.6% under the A2 (~ RCP8.5) wave scenario and 60.9% under the B2 (~RCP6.0) scenario. Thus, compared with the Baseline (status quo) scenario: both the A2 and B2 wave scenarios would reduce the proportion of Waimakariri River sand transported south (by virtue of relatively reduced wave energy from the northeast quarter); a rise in sea-level with no change in offshore wave climate would increase it; and under combinations of sea-level rise and wave climate change, while the two effects would compensate the wave climate change would prevail, resulting in reduced proportions transported south (63.7% for A2, 65.7% with B2).
- Beach profile closure depth:
 - While varying alongshore according to exposure to storm waves, the general pattern is for the closure depth to increase with sea-level rise (due to more wave energy incident on the shore), decrease under the A2 and B2 wave scenarios (due to reduced storm wave energy, more so under the A2 scenario), but not change much under combined sea-level rise and wave climate change scenarios.
 - An increased closure depth increases the sand volume required to lift the beach profile to match a rise in sea-level. This is because of the exponential shape of the nearshore profile (Equation 8, Figure 2-9), which means that the average slope of the profile (i.e., H/L in Equations 4, 5, and 6) reduces the deeper the closure depth point is positioned.
- Sand capture by the Avon-Heathcote inlet/ebb-delta system:
 - The net sand demand for enlarging the Avon-Heathcote Inlet ebb-delta and throat associated with rising sea-level could be anywhere between zero and 8% of the present (182,000 m³/yr) river sand supply rate to the City shore.

3.4.2 Effects on beach budget and shoreline position trends

Ten potential future combinations of the river-load/wave/sea-level changes listed above were selected to assess the range of effects on the beach sediment budget and spatially-averaged trends of shoreline movement for the Sumner to Waimakariri Mouth shore, using the spreadsheet budgeting model described in Section 2.4. These 10 combinations are defined in Table 3-9 and are compared with a Status Quo scenario that uses baseline values from the existing budget reported by Hicks et al. (2018).

The key results in Table 3-9 are found in the last two rows. The “Derived shore shift rate at 2120” (second bottom row) is calculated from Equation (6) using the data listed in the rows above¹². If the beach budget is in surplus, this figure is positive and the shore is advancing on average. Under the status quo, the calculated advance rate of 0.48 m/yr aligns well with the 1990-2017 average rate of shore advance of 0.46 m/yr derived by Hicks et al. (2018) from the ECan profiles.

The “SLR rate for a stable shore” (bottom row) is calculated from Equation (7) and shows what the rate of sea-level rise would need to be for the shoreline position to stabilise (i.e., neither advance or retreat). For the status quo case, this is a rise-rate of 12 mm/yr. The shore would begin to erode only when the rate of sea-level rise exceeded this rate.

The scenarios are ordered in Table 3-9 according to the derived shore shift rate, so the most hazardous scenario for shore erosion is on the left, and things get better to the right.

The shore would only be eroding significantly by 2120 (negative shore shift rates) under the “worst case” independent combinations of reduced river sand delivery, a reduced southwards distribution of river sand, inlet sand losses, and a 1.36 m extreme sea-level rise (associated with the 83rd percentile of sea-level projections under the extreme, “high emissions” RCP8.5 climate change scenario) – which are Scenarios A and B in Table 3 9.

Scenario C shows that when the RCP8.5 scenario effects are coupled (i.e., increased river sand load, 83rd percentile sea-level rise, wave climate change, inlet losses), the shore would be eroding at 0.09 m/yr. If there were no irrigation and inlet losses and no wave climate change associated with this extreme sea-level rise, the shore would be stable (Scenario D).

Using the median RCP8.5 sea-level trajectory (instead of the 83rd percentile trajectory), including irrigation and tidal inlet losses would result in a shore advance rate of 0.12 m/yr (Scenario E), while with zero irrigation and inlet losses the shore advance rate would be 0.18 m/yr (Scenario F).

For an RCP6.0 related scenario (Scenario G), with a smaller sea-level rise, the net river load increased by 9% (which is the mid-range of our estimates), and no inlet losses, the shore advance rate would 0.23 m/yr. For an RCP2.6 related scenario (Scenario H), with an even smaller sea-level rise, the net river load decreased by 11%, and no inlet losses, the shore advance rate would be 0.28 m/yr.

Even with the worst case RCP8.5 climate change scenario, a doubling of the river sand delivery due to earthquake-trigger landslides in the upper Waimakariri Catchment would maintain a shoreline advance rate of 0.33 m/yr (Scenario I). The same landslide effect under status quo conditions, without any climate change complications, would cause the shore to advance at over 1 m/yr (Scenario M).

In overview, the main finding is that at least until 2120 the City shore sand budget should remain in surplus (and the shore should not begin to erode) except under the worst case RCP8.5 climate change scenario (which couples the effects of changed Waimakariri River sand load, sand losses due to future irrigation takes, reduced southward wave-driven sand distribution from the river mouth, a 1.36 m sea-level rise, and sand losses to the ebb-delta at the Avon-Heathcote Inlet).

¹² In Table 3-9, the sea-level rise rate at 2120 for the various climate change scenarios was derived from Figure 24 of MfE (2017). Polynomial functions were fitted to the various sea-level projections, and these functions were differentiated to enable estimates of the rate-of-change in sea-level at future dates.

We caution that this is a spatially-averaged result for the shore between Sumner and the Waimakariri River mouth, while actual shoreline movements are likely to vary locally from the average rate. This is indicated by several lines of evidence, including:

- The alongshore pattern of historical shoreline shift indicated over recent decades by the ECan profile dataset (Figure 3-19 from Hicks et al. 2018).
- The alongshore pattern of accretion and erosion indicated by the divergence in longshore transport potential (Figure 3-7f).
- The results of the one-line numerical shoreline modelling study of Hicks (1993), which indicated that a reduction (by 50%) in the Waimakariri River sand supply would result in an approximately 10-km long erosion “bite” developing centred on the river mouth while the shore overall remained in sand surplus and continued to advance further south. This occurred because, effectively, the subtle shoreline ‘bulge’ that occurs at the Waimakariri River mouth was trimmed back. The modelling also showed the “bite” deepening and diffusing alongshore with time.

Numerical shore modelling would be required to explore the spatially-detailed shore response to the scenarios listed in Table 3-9. Such a model would need to capture beach changes out to the closure depth and be able to simulate both wave and current-driven transport processes, including the Avon-Heathcote inlet and ebb-delta and the Waimakariri River delta.

Table 3-9: Impacts of future sand budget scenarios on alongshore-averaged shoreline shift rate, Waimakariri to Sumner. Refer text for description of content. Asterisk indicates sea-level rise effects on waves estimated by interpolation.

Scenario label	A	B	C	D	E	F	G	H	I	J	K
Scenario description	Worst case independent combination	Worst case independent combination	RCP8.5 83 percentile SLR	RCP8.5 83 percentile SLR, no wave change, inlet loss	RCP8.5 Median* + ebb-delta losses	RCP8.5 Median*	RCP6.0	RCP2.6*	Landslide doubles river load	Status quo	Landslide doubles river load, no CC
River load scenario	Reduced 8% by CC, 3% by irrigation	Reduced 8% by CC, 3% by irrigation	Increased 28% by CC, reduced 3% by irrigation	Increased 28% by CC, zero irrigation effect	Increased 28% by CC, reduced 3% by irrigation	Increased 28% by CC, zero irrigation effect	Increased by 9%	Reduced 8% by CC, 3% by irrigation	Load doubled	Baseline	Load doubled
Waves scenario	B2	A2	A2	Baseline	A2	A2	B2	Baseline	A2	Baseline	Baseline
Sea-level rise by 2120 (m)	1.36	1.36	1.36	1.36	1	1	0.63	0.55	1.36	Baseline	Baseline
River sand load to tidal reach (million m ³ /yr)	0.664	0.664	0.933	0.955	0.933	0.955	0.813	0.664	1.492	0.746	1.492
River sand load to coast (million m ³ /yr)	0.653	0.653	0.922	0.944	0.924	0.947	0.807	0.659	1.481	0.744	1.490
Nearshore trap efficiency (%)	36%	36%	36%	36%	36%	36%	36%	36%	36%	36%	36%
Proportion moved south (%)	0.610	0.637	0.637	0.724	0.637	0.637	0.600	0.680	0.637	0.680	0.680
Losses to A-H ebb-delta (million m ³ /yr)	0.015	0.015	0.015	0	0.015	0	0	0	0.015	0	0
Shore span (km)	20.65	20.65	20.65	20.65	20.65	20.65	20.65	20.65	20.65	20.65	20.65
Average profile height (m)	15.10	14.80	14.80	15.35	14.75	14.75	14.84	14.70	14.80	15.07	15.07
Average profile width (m)	758	719	719	789	710	710	724	700	719	751.5	751.5
Sea-level rise rate at 2120 (m/yr)	0.015	0.015	0.015	0.015	0.011	0.011	0.007	0.005	0.015	0.002	0.002
Derived Shore shift rate at 2120	-0.341	-0.288	-0.086	0.005	0.117	0.183	0.228	0.275	0.333	0.485	1.072
SLR rate for a stable shore (m/yr)	0.008	0.009	0.013	0.015	0.013	0.015	0.012	0.011	0.022	0.012	0.023

3.5 Effects on Waimakariri River mouth stability

Boyle (2011) describes how the Waimakariri River's mouth was forced to its current location by engineering intervention in the 1930s; prior to that its outlet to Pegasus Bay was via what is now Brooklands Lagoon. Boyle also regarded the recent phase of erosion of the tip of Brooklands Spit as being associated with sand bar movements and was part of a cyclic process. We concur that this is the most likely explanation: sand bar movements and associated occasional redirecting of outflow channels and focussing of waves and currents onto spit tips are typical features of sandy river deltas on coasts exposed to moderate wave energy. Moreover, inspection of time-lapse satellite imagery¹³ of the mouth over the past 20 years confirms a cyclic behaviour.

The prevalence of southward over northward longshore transport past the river mouth could potentially be a factor forcing spit tip erosion, since, typically, river outflows tend to get deflected in the direction of the net longshore transport. However, at the Waimakariri River mouth, any such underlying tendency appears to be nullified by the rock revetment on the true left (northern) bank, which tends to keep the river in place beside the revetment rather than deflecting south.

Such cyclic behaviour at the river mouth should continue under the simulated future nearshore wave scenarios, since they show very little difference in the alongshore distribution of wave energy and longshore transport potential (Figure 3-7).

The risk appears small of waves over-washing Brooklands Spit and the Waimakariri suddenly re-locating its outlet through Brooklands Lagoon again. This is because of the accretional trend shown by the spit's ocean shore and the reasonable assumption that the height of the foredune field on the spit will grow in pace with rising sea-level. Even if a river break-out did occur at Brooklands, it is likely that ECan would re-engineer it back to its present location for flood control purposes.

The most likely source of large-scale river mouth instability would accompany the arrival and peak of a sand pulse following earthquake landslides in the upper catchment. With this, the river delta would enlarge, sand bars would become larger and more active, and interactions between bars and the shoreline would increase in amplitude as the delta became a "clearing house" for the additional sand. This behaviour would persist for 1-2 decades while the bulk of the landslide-sourced sand was being flushed into and down the river, with the size of the delta waxing and waning as a function of the occurrence of river floods (bringing the sand) and coastal processes (moving the sand onshore and alongshore). Possibly, another spit and foredune system could form seaward of the present one – as was inferred to have occurred with the earthquake-related beach ridges in South Westland (Wells and Goff 2007).

3.6 Effects on inundation

Given (from Section 3.4.2) that the City's open-ocean shore is likely to remain accretionary overall for the next century under all but the most extreme (RCP8.5) climate-change/sea-level rise scenario, then we do not consider it likely that coastal flooding of this shore will generally be exacerbated by shore erosion over that period. This assumes that as sea-level rises the foredune system will naturally increase in height, maintaining a barrier to storm wave overwash (and where there are seawalls instead of a foredune, we assume that these will be increased in height appropriately).

¹³ <https://earthengine.google.com/timelapse/>.

The exception will be at the Avon-Heathcote Inlet due to inlet widening as sea-level rises and the tidal prism increases.

Increased flooding should be expected, of course, around unprotected spans of the Avon-Heathcote Estuary (including the lower reaches of the Avon and Heathcote Rivers) and Brooklands Lagoon shores due to “bath-tub” inundation with rising sea-level, coupled with an increased risk of overtopping by local-fetch waves assisted by wind setup.

4 Conclusions

The main conclusions of this study are:

1. The Waimakariri River's future (by 2100) sand delivery to the tidal reach due to climate change effects and human responses could vary between a reduction of 11% on the current delivery (8% reduction from up-catchment associated with the "low emissions" RCP2.6 or RCP4.5 climate change scenarios and 3% interception by irrigation takes with no sand returns to the river) and a 28% increase (28% increase from up-catchment associated with the more extreme "high emissions" RCP8.5 climate change scenario and all irrigation-intercepted sand flushed back to the river). A "most likely" change in sand delivery rate could be taken at the mid-range of these bounds (i.e., a 9% increase), but the uncertainty around this figure should be appreciated.
2. Following a major future alpine earthquake, landslides (300 million m³ combined volume of which 20% renders to sand) clustering mainly in or just upstream of the Waimakariri Gorge would at least double (possibly treble) the river's sand load for over 10 years, with landslide sand first arriving at the coast within 1-2 years of the landslide event, and 90% of the landslides' coastal sand delivery occurring over 30 years. Dispersion of the landslide's sand pulse along the shore by coastal processes would likely occur slowly, with several decades elapsing before any signature appeared at Waimairi Beach and longer to reach Southshore.
3. Sea-level rise driven deposition in the tidal reach of the Waimakariri River would be 1,300 m³/yr under the status quo (sea-level rise rate of 2 mm/yr), 3,600 m³/yr with a rise-rate of 5.4 mm/yr, and 8,800 m³/yr with a rise-rate of 11 mm/yr, thus reducing the river sand delivery to the coast by these amounts.
4. Under sea-level rise and a climate-change altered nearshore wave climate, the proportion of river sand load transported south from the Waimakariri River mouth could change from the baseline estimate of 68%. Both the A2 (~RCP8.5) and B2 (~RCP6.0) wave scenarios would reduce the proportion of Waimakariri River sand transported south (by virtue of relatively reduced wave energy from the northeast quarter); a rise in sea-level with no change in offshore wave climate would increase it; and under combinations of sea-level rise and wave climate change, while the two effects would compensate the wave climate change would prevail, resulting in reduced proportions transported south.
5. Beach profile closure depth would increase with sea-level rise (due to more wave energy incident on the shore), decrease under the A2 and B2 wave scenarios (due to reduced storm wave energy), but not change much under combined sea-level rise and wave climate change scenarios. An increased closure depth increases the sand volume required to lift the beach profile to match a rise in sea-level.
6. The net sand demand for enlarging the Avon-Heathcote Estuary ebb-delta and throat associated with rising sea-level could be anywhere between zero and 8% of the present (~182,000 m³/yr) river sand supply rate to the City shore.
7. At least until 2120, the City shore sand budget should remain in surplus (and the shore should not begin to erode) except under the worst case RCP8.5 climate change scenario (which couples the effects of changed Waimakariri River sand load, sand losses due to future

irrigation takes, reduced southward wave-driven sand distribution from the river mouth, a 1.36 m sea-level rise, and sand losses to the ebb-delta at the Avon-Heathcote Inlet).

8. We caution that this is a spatially-averaged result for the shore between Sumner and the Waimakariri River mouth, while actual shoreline movements are likely to vary locally from the average rate. Numerical shore modelling would be required to develop spatially-detailed shore responses, and this modelling would need to capture beach changes out to the closure depth and be able to simulate both wave and current-driven transport processes, including at the Avon-Heathcote inlet and ebb-delta and the Waimakariri River delta.
9. Any significant future shore instability at the Waimakariri River mouth would likely accompany the arrival of a sand pulse following earthquake-triggered landslides in the upper Waimakariri Catchment. With this, the river delta would enlarge, sand bars would become larger and more active, interactions between bars and the shoreline would increase in amplitude, and possibly another spit and foredune system could form seaward of the present one. Otherwise, the recently-observed cycles of spit-tip erosion and bar changes should most likely continue. The risk of waves over-washing Brooklands Spit and the Waimakariri River suddenly re-locating its outlet through Brooklands Lagoon again is small, even under wave climate change and sea-level rise scenarios.
10. Given that the City's open-coast shore is likely to remain accretionary overall for the next century under all but the most extreme (RCP8.5) climate change and sea-level rise scenario, then we do not anticipate the risk of sea-flooding from the ocean-side will generally be exacerbated by shore erosion and sea-level rise. The exception will be at the southern tip of Southshore Spit due to the Avon-Heathcote Inlet widening as sea-level rises and the tidal prism increases.

5 Acknowledgements

We thank:

- Professor Tim Davies (University of Canterbury) for information and discussion around potential earthquake-induced landslides in the Waimakariri Catchment.
- Shaun McCracken and Tony Boyle (Environment Canterbury) for discussions on the likely ECan response to managing a Waimakariri River sediment slug.
- Drs Christian Zammit and Daniel Collins (NIWA) for providing simulated Waimakariri discharges under future climate change scenarios.
- Marion Schofield, Graham Harrington, and John Walter (Christchurch City Council) and Derek Todd (Jacobs) for review comments on an early draft of this report.

6 Glossary of acronyms

Delft3D	A two- or three-dimensional numerical hydrodynamical mode, developed by Deltares in The Netherlands, that simulates currents and water levels in rivers, estuaries, and coastal settings.
GCM	Global Climate Model. A numerical model that simulates global weather and is sensitive to atmospheric composition.
LDRP	Land Drainage Recovery Programme. A programme of investigation seeking to understand the post Christchurch Earthquake Sequence flood risk in the greater Christchurch area due to the co-location, coincidence, and cascading of multiple hazards.
RCM	Regional Climate Model. A model that downscales the output from a GCM to regional scales, taking account of local influences such as land topography.
RCP	Representative Concentration Pathway. A projected trajectory for future atmospheric greenhouse gas concentration based on an assumed human response to global warming (ranging from business-as-usual, with increasing emissions, to proactive reduction of gas emissions). Used as input to GCMs.
SRH-1D	Sedimentation and River Hydraulics - 1D. A one-dimensional hydraulic and morphological model, developed by the US Bureau of Reclamation, that simulates sediment transport and bed evolution along rivers.
SWAN	Surface Waves At Nearshore. A numerical model that generates wave spectra and/or is driven by wave spectra at an offshore/deep-water boundary, and refracts and shoals the wave spectra inshore.
TopNet	A distributed hydrological model that simulates catchment water balance and river runoff from input weather data.
WASP	Wave and Storm Surge Projections. A NIWA project to generate deep-water wave and storm surge predictions based on data output from an RCM coupled with GCMs. Used to estimate the effects of future climate change scenarios on local waves and storm surge.
Wavewatch III	A third-generation model that generates waves over the global oceans using wind data output from a GCM. Developed by the National Center for Environmental Prediction (NCEP) and the National Oceanic and Atmospheric Administration (NOAA), US.

7 References

- Adams J. (1981) Earthquake-dammed lakes in New Zealand. *Geology* 9(5): 215–219.
- Asselman, N.E.M., H. Buitenveld, M. Haasnoot, F.J.P.M. Kwaad, J.C.J. Kwadijk, H. Middelkoop, W.P.A. van Deursen, P.M. van Dijk, J.A. P.H. Vermulst, C. Wesseling (2000) The impact of climate change on the river Rhine and the implications for water management in the Netherlands. Summary report of the NRP project 952210, June 2000.
- Boyle, A.J. (2011) An investigation into the southward migration of the Waimakariri River mouth. Technical Report No. R11/121, Environment Canterbury, May 2011.
- Boyle, A.J., Surman, M.R. (2009) Waimakariri River bed level investigation. Environment Canterbury Report No. R08/11, ISBN 978-1-86937-758-8.
- Bruun, P. (1962) Sea level rise as a cause of shore erosion. *Journal of Waterway, Port, Coastal and Ocean Engineering*, American Society of Civil Engineers, 88, 117-130.
- Canterbury Mayoral Forum (2009) Canterbury Water Management Strategy. <https://www.ecan.govt.nz/document/download/?uri=2105939>.
- CCC (2017) Land Drainage Recovery Programme Coastal Sediment Budget Study. Project WBS: 561/238/113, TRIM Number: 17/1177561, LDRP 113, Tender version, October 2017.
- Collins, D.B.G., Zammit, C. (2016) Climate change impacts on agricultural water resources and flooding. *NIWA Client Report* No. 2016114CH, prepared for Ministry for Primary Industries, November 2016.
- Croissant, T., Lague, D., Steer, P., Davy, P. (2017) Rapid post-seismic landslide evacuation boosted by dynamic river width. *Nature Geoscience* 10(9):680–684.
- Dean, R. G. (1991) Equilibrium beach profiles: characteristics and applications. *Journal of Coastal Research*, 7(1), 53–84. <https://doi.org/10.2307/4297805>.
- Gelfenbaum, G., Stevens, A.W., Miller, I., Warrick, J.A., Ogston, A.S., Eidam, E. (2015) Large-scale dam removal on the Elwha river, Washington, USA: Coastal geomorphic change. *Geomorphology* 246: 649-668.
- Goff, J., McFadgen, B.G., Wells, A., Hicks, M. (2008) Seismic signals in coastal dune systems. *Earth Science Reviews* 89: 73-77.
- Gorman, R. M. (2016) Projected changes in New Zealand’s wave climate. Paper presented at the New Zealand Coastal Society 24th Annual Conference, Dunedin.
- Gorman, R., Bell, R.G. (2011) What’s happening to New Zealand’s wave climate? Paper presented at the New Zealand Coastal Society 19th Annual Conference, Nelson.
- Greimann, B., Huang, J.V. (2018) SRH-1D 4.0 User’s Manual, Sedimentation and River Hydraulics Group, Bureau of Reclamation, Denver Colorado.

- Hicks, D.M. (1993) Modelling long-term change of the Pegasus Bay shoreline. Report to Canterbury Regional Council. NIWA Christchurch Miscellaneous Report No. 27.
- Hicks, D.M., Gorman, R.M., Measures, R.J., Walsh, J.M., Bosserelle, C. (2018) Coastal sand budget for Southern Pegasus Bay: Stage A, *NIWA Client Report 2018062CH*. Prepared for Christchurch City Council.
- Hicks, D.M., Hume, T.M. (1996) Morphology and size of ebb-tidal deltas at natural inlets on open-sea and pocket-bay coasts, North Island, New Zealand. *Journal of Coastal Research* 12 (1): 47-63.
- Hicks, D.M., Inman, D.L. (1987) Sand dispersion from an ephemeral river delta on the Central California coast. *Marine Geology* 77: 305-318.
- Hicks, D.M., Shankar, U., McKerchar, A., Basher, L.R., Lynn, I, Page, M., Jessen, M. (2011) Sediment yield from New Zealand rivers. *Journal of Hydrology (NZ)* 50(1): 81-142.
- Hume, T.M., Herdendorf, C.E. (1988) The “Furkert-Heath” relationship for tidal inlet stability reviewed. *New Zealand Journal of Marine and Freshwater Research*, 22:1, 129-134, DOI: 10.1080/00288330.1988.9516284.
- Kidson, J.W. (2000) An analysis of New Zealand synoptic types and their use in defining weather regimes. *International Journal of Climatology* 20: 299-316.
- McFadgen, B.G., Goff, J.R. (2005) An earth systems approach to understanding the tectonic and cultural landscapes of linked marine embayments: Avon-Heathcote Estuary (Ihutai) and Lake Ellesmere (Waihora), New Zealand. *Journal of Quaternary Science* 20(3): 227–237.
- McSaveney, M., Davies, T. (2007) Rockslides and their motion. In: Sassa, K., Fukuoka, H., Wang, F., Wang, G. (eds) *Progress in Landslide Science*. Springer-Verlag., p 113–134.
- Measures, R. (2012) Modelling gravel transport, extraction and bed level change in the Waimakariri River, *NIWA Client Report CHC2012-121*. Environment Canterbury Report No. R12/128.
- Measures, R.J., Bind J. (2013) Hydrodynamic model of the Avon Heathcote Estuary: Model build and calibration, *NIWA Client Report CHC2013-116*.
- MfE (2008) Coastal Hazards and Climate Change. A Guidance Manual for Local Government in New Zealand. 2nd edition. Revised by Ramsay, D, Bell, R. (NIWA). Prepared for Ministry for the Environment. viii+127 p.
- MfE (2016a) Climate Change Projections for New Zealand: Atmosphere Projections Based on Simulations from the IPCC Fifth Assessment. Ministry for the Environment, Wellington.
- MfE (2016b) Climate Change Projections for New Zealand – Snapshot June 2016 Info 765. Ministry for the Environment, Wellington.
- MfE (2017) Coastal hazards and climate change: Guidance for local government. Publication number: ME 1341, Ministry for the Environment, Wellington.

- Mullan, A.B., Sood, A., Stuart, S. (2016) Climate change projections for New Zealand based on simulations undertaken for the IPCC 5th Assessment. Part A: Atmosphere Changes. NIWA Client Report for Ministry for the Environment, WLG2015-31. June 2016.
- Orchard, S., Measures, R.J. (2017) Sea level rise impacts in the Avon Heathcote Estuary Ihutai Salinity intrusion and inanga spawning scenarios, Waterlink Ltd report for Christchurch City Council.
- Smart, G.M., Mullan, A.B., Henderson, R. (2018) Coincident Inclement Weather Study for climate change planning. *NIWA Client Report* 2018095CH, prepared for Christchurch City Council., May 2018.
- Tonkin & Taylor (2017) Coastal Hazard Assessment. Report prepared for Christchurch City Council, November 2017.
- Waimakariri Zone Committee (2012) Waimakariri Zone Implementation Programme. <https://www.ecan.govt.nz/document/download/?uri=2138529>.
- Walters, R.A., Goring, D.G., Bell, R.G. (2001) Ocean tides around New Zealand. *New Zealand Journal of Marine and Freshwater Research* 35(3): 567–579.
- Wells, A., Goff J. (2007) Coastal dunes in Westland, New Zealand, provide a record of paleoseismic activity on the Alpine fault. *Geology* 35(8): 731–734.
- Woods, R., Hendrikx, J., Henderson, R., Tait, A. (2006) Estimating mean flow of New Zealand rivers. *Journal of Hydrology (NZ)* 45: 95-110.
- Wu, W., Wang, S.S.Y., Jia, Y. (2000) Nonuniform sediment transport in alluvial rivers. *Journal of Hydraulic Research* 38(6): 427–434.
- Zammit, C., Woods, R.A. (2011) Projected climate and river flow for the Waimakariri catchment for 2040s and 2090, *NIWA Client Report* no CHC 2011-25, 52p.

Appendix A Kidson Weather Types

Kidson (2000) defined 12 synoptic weather types with characteristic atmospheric circulation patterns over New Zealand (Figure A-1). These were organised into three groups or “regimes”. The “trough” regime relates to unsettled conditions; the “zonal” regime has westerly flow over the country; while the “blocking” regime is characterised by anticyclones with generally settled weather.

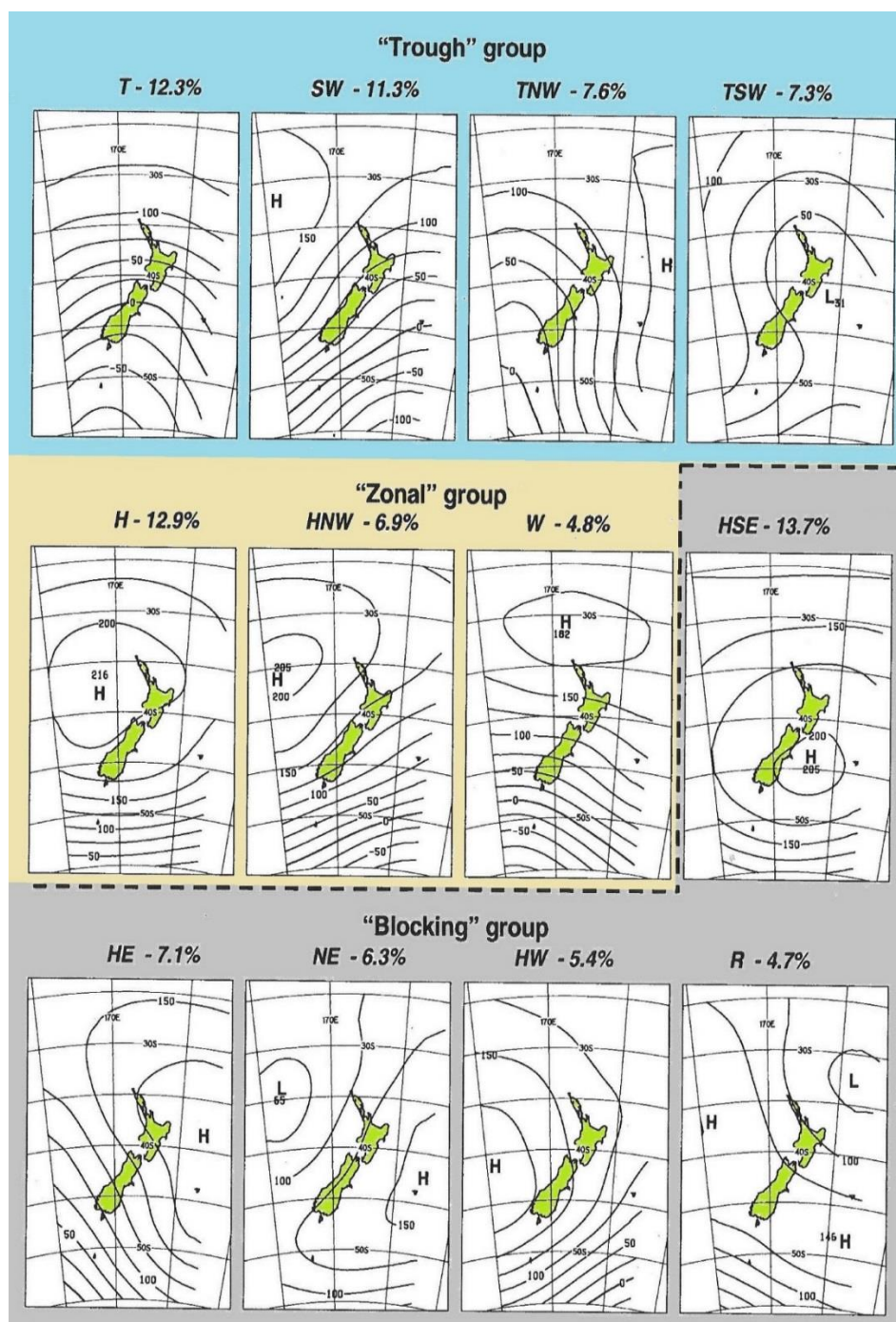


Figure A-1: The twelve Kidson Weather Types represented as anomalies in the 1000 hPa geopotential height. The symbol identifying the type (e.g., T, SW, TNW, etc.) is shown above each map. The types are organised into a “Trough” group, a “Zonal” group, and a “Blocking” group. The percentages next to the type identifier represent the observed frequencies of each type, as determined by Kidson (2000) using 1958-1997 data. Reproduced from Smart et al. (2018).

Appendix B WASP wind scaling

Wind inputs to the SWAN model associated with the future climate change scenarios were scaled onto the measured wind record using a linear transformation of the vector wind components. Such a linear transformation can be expressed as

$$\begin{bmatrix} u' \\ v' \end{bmatrix} = \begin{bmatrix} \bar{u}' \\ \bar{v}' \end{bmatrix} + \begin{bmatrix} a & 0 \\ 0 & b \end{bmatrix} \begin{bmatrix} \cos \theta & \sin \theta \\ -\sin \theta & \cos \theta \end{bmatrix} \begin{bmatrix} u - \bar{u} \\ v - \bar{v} \end{bmatrix} \quad (\text{B-1})$$

This involves successively subtracting the mean components \bar{u} and \bar{v} , rotating by an angle θ , then separately scaling the new components before adding back the mean of the transformed components.

Starting from time series of velocity components from a WASP simulation, we can perform the first two of these steps, omitting the scaling factors for now, to identify a principle axis of alignment of the winds by choosing the rotation angle θ that maximises the standard deviation σ_{prin} of the principal component u' and minimises the standard deviation σ_{trans} of the transverse component v' . This provides five characteristic parameters for each wind record: \bar{u} , \bar{v} , θ , σ_{prin} , σ_{trans} .

If we now set $a = 1/\sigma_{prin}$ and $b = 1/\sigma_{trans}$, the resulting u' and v' are normalised variables with zero mean and standard deviation 1.

The inverse of the above linear transformation is

$$\begin{bmatrix} u \\ v \end{bmatrix} = \begin{bmatrix} \bar{u} \\ \bar{v} \end{bmatrix} + \begin{bmatrix} \cos \theta & -\sin \theta \\ \sin \theta & \cos \theta \end{bmatrix} \begin{bmatrix} 1/a & 0 \\ 0 & 1/b \end{bmatrix} \begin{bmatrix} u' - \bar{u}' \\ v' - \bar{v}' \end{bmatrix} \quad (\text{B-2})$$

We computed these parameters (Table B-1) for the baseline simulation and each futurecast (in the case of A2, we can compute a single parameter set from combining the three realisations). Given an input wind record as used in the “present day” SWAN simulation, we then transform it for a “climate change” simulation by:

- Applying the forward transformation (B-1) using the parameters from the WASP baseline to produce normalised components.
- Applying the inverse transformation (B-2) to the resulting normalised components using the parameters from the relevant WASP futurecast.

Table B-1: Wind climate parameters from the WASP simulations. b.

	θ	\bar{u}	\bar{v}	σ_{prin}	σ_{trans}
	radians	m/s	m/s	m/s	m/s
Baseline	1.1295372	-0.066	0.113	6.438	3.052
B2	1.1382465	-0.213	-0.239	6.477	3.083
A2	1.1539378	-0.120	-0.210	6.472	3.122